Modeling the reactive halogen plume from Ambrym volcano and its impact on the troposphere with the CCATT-BRAMS mesoscale model

L. Jourdain, Tjarda J Roberts, M. Pirre, B. Josse

Atmos. Chem. Phys. Discuss., 15, 35313–35381, 2015
www.atmos-chem-phys-discuss.net/15/35313/2015/
doi:10.5194/acpd-15-35313-2015

Atmospheric Chemistry and Physics Discussions
Open Access
EGU

Modeling the reactive halogen plume from Ambrym volcano and its impact on the troposphere with the CCATT-BRAMS mesoscale model

L. Jourdain[1], T. J. Roberts[1], M. Pirre[1], and B. Josse[2]

[1]Laboratoire de Physique et de Chimie de l'Environnement et de l'Espace (LPC2E), Université d'Orléans, CNRS, Orléans, France
[2]CNRM-GAME, Météo-France and CNRS, Toulouse, France

Received: 31 July 2015 – Accepted: 21 November 2015 – Published: 16 December 2015

Correspondence to: L. Jourdain (line.jourdain@cnrs-orleans.fr)

Published by Copernicus Publications on behalf of the European Geosciences Union.

Abstract

Ambrym volcano (Vanuatu, Southwest Pacific) is one of the largest sources of continuous volcanic emissions worldwide. As well as releasing SO_2 that is oxidized to sulfate, volcanic plumes in the troposphere are shown to undergo reactive halogen chemistry whose atmospheric impacts have been little explored to date. Here, two-way nested simulations were performed with the regional scale model CCATT-BRAMS to test our understanding of the volcano plume chemical processing and to assess the impact of Ambrym on atmospheric chemistry at local and regional scales. We focus on an episode of extreme passive degassing that occurred in early 2005 and for which airborne DOAS measurements of SO_2 and BrO columns, in the near downwind plume, have been reported. The model was developed to include reactive halogen chemistry and a volcanic emission source specific to this extreme degassing event. SO_2 simulated columns show very good quantitative agreement with the DOAS observations as well as with OMI data, suggesting that the plume direction as well as its dilution are well represented. Simulations are presented with and without a high-temperature initialization that includes radicals formed by high temperature partial oxidation of magmatic gases by ambient air. When included high-temperature chemistry initialization, the model is able to capture the observed BrO/SO_2 trend with distance from the vent in the near downwind plume. However, the maximum of BrO columns enhancement is still underestimated by a factor 3. The model identifies total in-plume depletion of ozone (15 ppbv) as a limiting factor to the partitioning of reactive bromine into BrO, of particular importance in this very strong plume at low background ozone conditions. Impacts of Ambrym in the Southwest Pacific region were also evaluated. As the plume disperses regionally, reactive halogen chemistry continues on sulfate aerosols produced by SO_2 oxidation and promotes BrCl formation. Ozone depletion is weaker than at local scale but still between 10 to 40 %, in an extensive region few thousands of kilometres from Ambrym. The model also predicts transport of bromine to upper troposphere and

ACPD
15, 35313–35381, 2015

stratosphere associated with convection events. In the upper troposphere, HBr is reformed from Br and HO_2.

The model confirms the potential for volcanic emissions to influence the oxidizing power of the atmosphere: methane lifetime (calculated with respect to OH and Cl) is overall increased in the model due to the volcanic emissions. Reactive halogen chemistry is responsible for about 62 % of the methane lifetime increase with respect to OH, with depletion of OH by SO_2 oxidation responsible for the remainder (38 %). Cl radicals produced in the plume counteract 41 % of the methane lifetime lengthening due to OH depletion. The reactive halogen chemistry in the plume is also responsible for an increase of 36 % of the SO_2 lifetime with respect to oxidation by OH. This study confirms the strong influence of Ambrym emissions during the extreme degassing event of early 2005 on the composition of the atmosphere at the local and regional scales. It also stresses the importance of considering reactive halogen chemistry when assessing the impact of volcanic emissions on climate.

1 Introduction

Volcanic activity is a source of climatically and environmentally important gases and aerosols in the atmosphere. To this respect, much work has been focusing on the climate impact of major volcanic explosions that inject directly and massively sulfur compounds into the stratosphere. In this layer, the sulfate aerosols have a long residence time (~ 1–2 years) and can affect climate directly via the perturbation of the Earth's radiation balance as well as indirectly due to the strong coupling between radiation, microphysics and atmospheric chemistry in the stratosphere. This forcing from volcanic stratospheric aerosols is now well understood and is thought to be the most important natural cause of externally forced climate change on the annual but also on the multidecadal time scales and hence can explain the majority of the pre-industrial climate change of the last millennium (Myrhe at al., 2013). On the other hand, because of the lower lifetime of volcanic emissions in the troposphere, the climate impact of quiescent

ACPD
15, 35313–35381, 2015

degassing and minor eruptions has been less studied. However, quiescent degassing alone is responsible for a high proportion (~ 30–70 %) of the volcanic SO_2 flux to the atmosphere (Andres and Kasgnoc, 1998; Halmer et al., 2002; Mather et al., 2003). In addition, quiescent degassing as well as minor eruptions were found to contribute more to the sulfur load in the free troposphere in regard to their emissions compared to stronger sources as oceanic and anthropogenic sources due to the elevation of most volcanoes (e.g., Chin and Jacob, 1996; Graf et al., 1997). Furthermore, recent studies show the need for a better knowledge of the tropospheric concentrations of natural aerosols and their precursor gases to quantify the aerosol indirect forcing from anthropogenic activities due to nonlinearities in the relations linking aerosol concentrations and cloud albedo (Carslaw et al., 2013; Schmidt et al., 2012). Volcanic emissions in the troposphere have also been recognized to cause environmental and health problems due to the deposition of SO_2, sulfate, hydrogen halides (mainly HCl and HF) and toxic metals (for a review, see Delmelle, 2003) as well as adversely impacting air quality. Moreover, there is evidence of chemical reactivity in tropospheric plumes with consequences on the oxidizing power of the troposphere (and hence effects on the climate) as well as on the deposition of mercury (e.g., von Glasow, 2010). Indeed, reactive halogen as BrO (e.g., Bobrowki et al., 2003; Lee et al., 2005; Oppenheimer et al., 2006; Bobrowski and Platt, 2007; Bani et al., 2009; Kern et al., 2009; Theys et al., 2009; Boichu et al., 2011; Kelly et al., 2013; Hörmann et al., 2013; Bobrowski et al., 2015) as well as OClO (Bobrowski et al., 2007; General et al., 2014; Gliß et al., 2015) have been detected in the plume of many volcanoes worldwide. Observations of ClO have also been reported (Lee et al., 2005) but are subject to some uncertainties (see Roberts et al., 2009). For BrO, it is clear that its formation results from the conversion of the emitted volcanic HBr gas into reactive bromine in the presence of sulfate aerosols (Oppenheimer et al., 2006; Bobrowski et al., 2007; Roberts et al., 2009; Von Glasow, 2010). The plume atmospheric chemistry is also highly influenced by the degree of plume mixing with entrained ambient air (Roberts et al., 2014a). Central to this chemical mechanism, first identified in the context of arctic spring ozone depletion event (Fan

ACPD
15, 35313–35381, 2015

and Jacob, 1992), is the reactive uptake of HOBr in the sulfate aerosol. The net result is bromide release from the sulfate aerosol to form gaseous reactive bromine (initially as Br_2, which then converts into other forms including Br, BrO, HOBr, $BrONO_2$) and depletion of oxidants O_3, HO_2 as well as NO_2. Reactive bromine acts as a catalyst to its own formation, leading to an exponential growth called "bromine explosion" also observed in the arctic during spring (e.g., Barrie et al., 1988), in the marine boundary layer (e.g., Saiz Lopez et al., 2004) and over salt lakes (e.g., Hebestreit et al., 1999) (for review see Simpson et al., 2015). Following the first discovery of volcanic BrO (Bobrowski et al., 2003), depletion of ozone has also been observed in volcanic plumes (Vance et al., 2010; Oppenheimer et al., 2010; Schuman et al., 2011; Kelly et al., 2013; Surl et al., 2015). Owing to the numerous environmental and climate impacts of quiescent degassing and minor eruptions occurring in the troposphere, it is important to take these volcanic sources into account in the 3-D atmospheric models (regional and global models) that aim to understand the chemical composition of the atmosphere, its evolution and its interaction with climate. This paper is an attempt to do that and builds on previous modeling work. The numerical 1-D models MISTRA and PlumeChem (e.g., Bobrowski et al., 2007; Roberts et al., 2009, 2014a; von Glasow et al., 2010; Boichu et al., 2011; Kelly et al., 2013) are able to reproduce observations of the ratios of BrO to SO_2 with distance from the craters volcanoes as well as simulate ozone depletion (e.g., Roberts et al., 2014a; Surl et al., 2015). These modeling studies show the need to take into account the high temperature chemistry following the mixing of volcanic gas with ambient air in order to reproduce the timing of BrO formation. Indeed, high-temperature model studies (Gerlach, 2004; Martin et al., 2006, 2009) have predicted that the mixing of volcanic gases and air at the vent leads to high temperature oxidative dissociation and hence to the formation of radical species. These species accelerate the onset of this chemistry, the formation of BrO being autocatalytical and driven forwards by reactions occurring on volcanic aerosol. To date, simulations of reactive halogen (BrO_x, ClO_x) chemistry in volcanic plumes and its impacts have been restricted to 1-D and box model studies.

ACPD
15, 35313–35381, 2015

Here, we present a 3-D regional model study of the impact of Ambrym volcano emissions, not only of sulfur emissions but also of halogen emissions including their reactive chemistry, on the chemical composition of the troposphere at both local and regional scales. Ambrym volcano, Vanuatu, is recognized as a significant contributor to the global volcanic flux of SO_2 (Bani et al., 2012; Allard et al., 2009, 2015) as well as of halogen halides HF, HCl, HBr (Allard et al., 2009, 2015). Our focus is an extreme degassing episode that occurred in early 2005, for which airborne DOAS SO_2 and BrO columns in the plume (15–40 km of the vents) have been reported (Bani et al., 2009).

The paper is organised as follows. In Sect. 2, we present the Ambrym volcano, the reported measurements and detail the model developments made in this study. In Sect. 3, we first test our understanding of the plume chemistry at the plume level by comparing the model simulations with the DOAS SO_2 and BrO columns in the near downwind plume and performing some sensitivity studies. The local impact of Ambrym plume is also presented. In Sect. 4, the regional impact of Ambrym plume is calculated and discussed. The conclusion is presented in Sect. 5.

2 Methods

2.1 Ambrym volcano

The Vanuatu Arc is a group of about 80 islands and islets located in the Southwest Pacific that was formed and had continued to evolve as a result of the complex interaction between the Pacific plate and the Indo-Australian plate (Robin et al., 1993). Ambrym (160°08′ E, 16°15′ S) situated in the central zone of the Vanuatu arc is a basaltic stratovolcano of 50 km long and 35 km wide rising 1334 m a.s.l. It has in its center a 12 km diameter caldera with two active cones Mounts Marum and Benbow filled with permanent lava lakes. It has been recently highlighted that the Vanuatu arc is one of the most important entry point for volcanic gases into the atmosphere with mean annual emission of 3 Tg yr^{-1} of SO_2 estimated for the period 2004–2009 representing about 20 %

ACPD
15, 35313–35381, 2015

of the global volcanic SO_2 annual emissions estimate (Bani et al., 2012). Under normal quiescent degassing conditions, Ambrym volcano has a mean emission of 5.44 kt day^{-1} of SO_2, comparable with Mt Etna (Italy), and hence contributes to two-thirds of the total budget of the arc (Bani et al., 2012). It is also a significant contributor to the global volcanic flux for several other species (Allard et al., 2009, 2015). The volcano impact on the population and environment includes crop damage and food shortages due to deposition of halogen acids, SO_2 and H_2SO_4 as well as dental fluorosis due to the water contamination by wet deposition of fluorine (Allibone et al., 2010). The volcano impact on sulfate aerosol in the Southwest Pacific has also recently been investigated (Lefèvre et al., 2015). They found a strong signal in the aerosol optical depth (AOD) from MODIS (Moderate Resolution Imaging Spectroradiometer) due to Ambrym sulfur emissions; this signal contributes for 15 % to the total AOD as far as 1500 km from the volcano. Here, we focus on the halogen impact alongside sulfur. We study an event of extreme passive degassing that took place in January 2005 when the SO_2 emission was more than 3 times higher that its mean value over the 2004–2009 period (Bani et al., 2012). This extreme degassing occurred as a pulse of several months duration (Bani et al., 2012). Our study evaluates impacts from the continuous degassing on 12 January, enabling comparison to plume BrO and SO_2 measurements from a field campaign (Bani et al., 2009).

2.2 Measurements

2.2.1 DOAS data

We use DOAS (Differential Optical Absorption Spectroscopy) measurement of SO_2 and BrO columns performed in the plume of Ambrym during the episode of extreme passive degassing the 12 January 2005 (Bani et al., 2009). The measurements were made between 05:00 and 06:00 UT onboard of an aircraft flying just below the Ambrym plume (at 500–1000 m a.s.l.) in the cross-wind direction (15–40 km south east of the craters) with the instrument's telescope pointing to zenith. The procedure to retrieve the

ACPD
15, 35313–35381, 2015

columns is described in Bani et al. (2009, 2012). Reported errors (2σ) on the SO_2 and BrO retrieved columns are respectively $\pm 52\,mg\,m^{-2}$ (i.e. 4.89×10^{16} molecules cm^{-2}) and $\pm 0.39\,mg\,m^{-2}$ (i.e. 2.44×10^{14} molecules cm^{-2}). In the present study, these data are used to evaluate the simulation of volcanic plume chemistry. Note that these data in conjunction with wind estimates were used by Bani et al. (2009) to estimate Ambrym SO_2 emission rate (18.8 kt day^{-1}).

2.2.2 OMI data

The Ozone Monitoring instrument (OMI) is a nadir viewing UV/visible CCD spectrometer sampling a swath of 2600 km with a ground footprint of 13 km × 24 km, launched aboard the NASA's Aura satellite in July 2004 (Bhartia and Wellemeyer, 2002). Here, we use the planetary boundary layer (PBL) level-2 SO_2 column amount product derived with the principal component analysis (PCA) algorithm (Li et al., 2013). Only data with scenes near the center of the swath (rows 5–55) with radiative cloud fraction less than 0.3 and with ozone slant column lower than 1500 DU were considered as recommended. Noise and biases in retrievals are estimated at ~ 0.5 DU for regions between 30° S–30° N.

2.3 Model description and simulations

We use the CCATT-BRAMS (Coupled Chemistry Aerosol-Tracer Transport model to the Brazilian developments on the Regional Atmospheric Modeling System, version 4.3) non-hydrostatic regional atmospheric chemistry model (described in detail in Longo et al., 2013). It is based on the Regional Atmospheric Modeling System (RAMS) developed by University of Colorado for a range of applications: from large eddy simulations in the planetary boundary layer to operational weather forecasting and climate studies (Walko et al., 2000). BRAMS builds upon RAMS and includes modifications and new features to improve the model performances within the tropics (Freitas et al., 2009). The parameterizations of physical processes such as surface–air exchanges, turbulence,

ACPD
15, 35313–35381, 2015

convection, radiation and cloud microphysics are described in Freitas et al. (2009) and in Longo et al. (2013). BRAMS is coupled on-line to CCATT that enables transport, chemical evolution, emission and deposition of chemical and aerosol species (Longo et al., 2013). Note that when BRAMS and CCATT are coupled, as in the present study, the prognostic chemical fields, O_3, N_2O, CO_2, CH_4 are used in the radiation scheme. The model has already been used to study regional air pollution, for instance: the South America regional smoke plume (Rosario et al., 2013) and ozone production and transport over the Amazon Basin (Bela et al., 2015). It has also been used to assess the transport of tropospheric tracers by tropical convection (Arteta, 2009a, b) and for understanding the budget of bromoform (Marécal et al., 2012).

The CCATT model is described in detail by Longo et al. (2013). Here we focus on the particular settings of the model we used and the changes we made for the study.

2.3.1 Model chemistry

Within the CCATT model, we use the RACM chemistry scheme (Regional Atmospheric chemistry Mechanism, Stockwell et al., 1997) including 88 species and 237 chemical reactions and designed to study tropospheric chemistry from urban to remote conditions. Photolysis rates are calculated on-line during the simulation to take into account the presence of aerosols and clouds using Fast-TUV (Tropospheric ultraviolet and visible radiation model, Tie et al., 2003; Longo et al., 2013). The sulfur scheme includes gas-phase oxidation, and dry and wet deposition, but not aqueous-phase oxidation. In order to simulate halogen chemistry in volcanic plumes, we have added to the chemical scheme 16 halogen species and 54 reactions including photolysis, gas phase and heterogeneous reactions. The gas phase constant rates and photolysis cross-sections are from JPL (Sander et al., 2006) and IUPAC (Atkinson et al., 2007). The heterogeneous reactions include the hydrolysis of $BrONO_2$ and the reaction of $HOBr + X^-_{(aq)} + H^+_{(aq)}$ where X = Br or Cl on sulfate aerosol. They are treated here with reactive uptake formulation (Table 1) with constant uptake coefficient. Ongoing developments are being made to prescribe a variable reactive uptake coefficient for HOBr as function of the

ACPD
15, 35313–35381, 2015

underlying gas-aerosol reaction kinetics, building on a recent re-evaluation (Roberts et al., 2014b).

For the heterogeneous reaction of $HOBr_{(g)}$ with $X^-_{(aq)}$ where X = Br or Cl, there is a subsequent inter-conversion between the products Br_2 and BrCl within the aerosols, based on the equilibria (Wang et al., 1994):

$$BrCl_{(aq)} + Br^-_{(aq)} \overset{K_1}{\longleftrightarrow} Br_2Cl^-_{(aq)} \tag{1}$$

$$Br_2Cl^-_{(aq)} \overset{K_2}{\longleftrightarrow} Br_{2(aq)} + Cl^-_{(aq)} \tag{2}$$

As a result, the relative amount of Br_2 and BrCl produced and released into the atmosphere depends on the equilibrium established by these two reactions. The Br_2/BrCl ratio is given by Eq. (3) (derived from equilibria of Wang et al., 1994):

$$\frac{[Br_{2(aq)}]}{[BrCl_{(aq)}]} = \frac{K_1}{K_2}\frac{[Br^-_{(aq)}]}{[Cl^-_{(aq)}]} \tag{3}$$

where the equilibrium constants of Eqs. (1) and (2) are $K_1 = 1.8 \times 10^4\,M^{-1}$ and $K_2 = 1.3\,M^{-1}$ respectively and the amounts of $[Br^-]$ and $[Cl^-]$ in the aqueous phase are determined by the effective Henry's law constants (taken from Sander, 1999). We thus parameterize the reactive uptake coefficient of HOBr as two competing reactions (with Br^- and Cl^-) and, on the basis of Eq. (3), apply a branching ratio to the constant rates of reactions as shown in Table 1. This approach is the same as that proposed by Grellier et al. (2014), and also similar to Roberts et al. (2014a) that showed competition between Br_2 and BrCl as products from HOBr reactive uptake, finding Br_2 is initially formed but BrCl becomes more prevalent once HBr becomes depleted. Note that heterogeneous reactions involving HOCl and $ClONO_2$ are slow compared to the reactions involving HOBr and $BrONO_2$ and are not taken into account in the model.

ACPD
15, 35313–35381, 2015

2.3.2 Sulfate aerosol surface density

In the model, sulphuric acid H_2SO_4 is a prognostic variable and assumed to be in totally in the aerosol phase. It is both directly emitted by the volcano (see Sect. 2.3.3 for details) and produced by the reaction of SO_2 with OH in the gas phase. We assume to have only binary H_2SO_4-H_2O aerosol. Weight percent of H_2SO_4 in the aerosol (wt) and the density of aerosols (ρ_{aer}) are calculated with the analytical expression of Tabazadeh et al. (1997) depending on the temperature and relative humidity. Total volume of aerosol V_{aer} (cm^{-3}) can then be calculated from H_2SO_4 concentrations, wt and ρ_{aer}. Few observations of volcanic aerosol size distribution exist, and none have been reported for Ambrym volcano plume. We assumed that the aerosols size follows a log-normal distribution with a fixed median diameter ($D_{median} = 0.5\,\mu m$) and a fixed geometric standard deviation ($\sigma = 1.8$). On this basis, the number of aerosol particles was deduced from V_{aer}, D_{median} and σ and the total aerosol surface densities ($cm^2\,cm^{-3}$) was then calculated (further details on lognormal aerosol distributions can be found in Seinfeld and Pandis, 2006). Here, the resulting surface area distribution has a surface median diameter of 1 µm and a maximum surface area of 7000 $\mu m^2\,cm^{-3}$ in the near-downwind plume and will be discussed in the results section.

Ongoing developments are being made to improve the volcanic aerosol representation to include two modes with diameter varying with hygroscopy, based on recent observations (Roberts et al., 2015).

2.3.3 Emissions

To generate the emissions, we have used the preprocessor PREP_CHEM_SRC (version 4.3) code described in detailed in Freitas et al. (2011). Anthropogenic emissions were prescribed using the RETRO (REanalysis of the TROposhperic chemical composition) global database (Schultz et al., 2007). Fire emissions were estimated using the Global Fire Emissions Database (GFEDv2) with $1^\circ \times 1^\circ$ spatial resolution and a 8 day temporal resolution (van der Werf et al., 2006). Biogenic emissions were provided by

ACPD
15, 35313–35381, 2015

a monthly climatology for the year 2000 produced with the MEGAN (Model of Emissions of Gases and Aerosols from Nature; Guenther et al., 2006) database. Details on the treatment of volcanic emissions and its modification for this study are given in the following.

SO_2 emissions

In CCATT-BRAMS, volcanic SO_2 emission rates are prescribed using the AEROCOM (Aerosol Comparisons between Observation and Models) database (Diehl et al., 2012; Freitas et al., 2011). This database includes volcanoes listed in the Smithsonian Institution's Global Volcanism Program database (GVP) (Siebert et al., 2010). Their emissions rates are assigned depending on their eruptive state (pre-eruptive, intra-eruptive, post-eruptive and extra-eruptive degassing), on their Volcanic Explosive Index (VEI) in case of eruption, and on additional information from TOMS (Total Ozone Mapping Spectrometer), OMI instruments and COSPEC (Correlation spectrometer) measurements) when available (Diehl et al., 2012).

Here, we replaced the values from the AEROCOM database for volcanoes of the Vanuatu Arc by more relevant information, when they were available. In particular, SO_2 emission rate for Ambrym (18.8 kt day^{-1}) is reported by Bani et al. (2009, 2012), using DOAS measurements (described in Sect. 2.2.1) in conjunction with wind-speed estimates. The error on this source is about ±20 % according to Bani et al. (2009).

SO_2 emissions rates of the most important volcanoes of the Vanuatu Arc in January 2005 are summarized in Table 2. Note that the Bagana volcano (6.140° S, 155.195° E, alt = 1750 m) in Papua New Guinea was also in activity for the period of the simulation, with an emission of 3.3 kt day^{-1} of SO_2 according to the AEROCOM database.

ACPD
15, 35313–35381, 2015

HBr and HCl emissions

HBr and HCl emission rates are derived from the measurements of HBr, HCl and SO_2 average fluxes reported for Ambrym by Allard et al. (2009). These average fluxes were based on airborne DOAS (to determine SO_2 flux) combined with gas ratios (to SO_2) calculated from crater-rim deployments of filter-pack samplers (for HBr, HCl, HF and/with SO_2) and Multi-Gas sensors (for CO_2, H_2O and/with SO_2), and are representative of a mean volcanic emission of Ambrym (P. Allard, personal communication, 2015). We did not use directly the HBr and HCl measurements but instead derived the HBr/SO_2 and HCl/SO_2 mass ratios (8.75×10^{-4} and 0.1, respectively) from the reported fluxes and applied them to our January 2005 SO_2 emission rate value to estimate the HBr and HCl emissions specifically for this date. Indeed, volcanic emission fluxes can vary with time. Allard et al. (2009) mean reported SO_2 emission rate for instance totals 8.8 kt day^{-1}, about two times smaller than the SO_2 emission rate reported during the extreme passive degassing event of 18.8 kt day^{-1}, but in closer agreement though with the estimate by Bani et al. (2012) of Ambrym mean activity of 5.4 kt day^{-1} for the period 2004–2009. The calculation yields HCl and HBr emissions of 1.9 kt day^{-1} and 16.5 t day^{-1}. Of note, the HBr/SO_2 and HCl/SO_2 mass ratios are close to (for HBr/SO_2 perhaps somewhat higher than) mean estimates for volcanic degassing as reported by Pyle and Mather (2009), but due to the high Ambrym SO_2 flux they yield very high volcanic halogen fluxes. By comparison, the Br flux from Mt Etna is reported as only 0.7 kt yr^{-1} (Aiuppa et al., 2005) i.e. 1.8 t day^{-1}, almost 10 times smaller. Note also that HF emissions were not considered in this study: whilst deposition impacts from HF around Ambrym can be severe (Allibone et al., 2010), HF does not contribute to reactive halogen cycling in the atmosphere (prevented by the strong H-F bond).

ACPD
15, 35313–35381, 2015

Sulfate emissions

We assume that 1 % of the sulphur (= $SO_2 + H_2SO_4$ here) is emitted as H_2SO_4 aerosol based on reported observations from several filter-pack studies at different volcanoes worldwide (e.g., Mather et al., 2003; Von Glasow et al., 2009, and references therein).

Initialisation with output from HSC Chemistry thermodynamic model

As mentioned earlier (see Sect. 1), the mixing of volcanic gas with ambient air at the vent leads to high temperature oxidative dissociation processes and hence to the formation of radical species. To take into account this high temperature chemistry, the thermodynamic model HSC Chemistry (Roine, 2007) was applied to simulate the equilibrium chemical composition of the volcanic gas-air mixture assuming a 98 : 2 volcanic gas : atmospheric gas composition. This approach follows that of previous 1-D model studies (Bobrowski et al., 2007; Roberts et al., 2009, 2014a; Von Glasow, 2010; Kelly et al., 2013; Surl et al., 2015). The model temperature was based on mixing an atmospheric temperature of 20 °C (consistent with that predicted by the CCATT-BRAMS model) and the magmatic degassing temperature of 1125 °C estimated by Sheehan and Barclay (2015). This was based on calculation of crystallisation temperatures of mineral phases in scoria samples collected from Ambrym in 2005, following models of Putirka (2008). The HSC Chemistry model input composition, shown in Table 3, is a 98 : 2 mixture of magmatic gases (with composition based on Allard et al., 2009), and atmospheric gases (78 % N_2, 21 % O_2, 1 % Ar). Roberts et al. (2014a) identifies key new species in the HSC Chemistry output as Br, Cl, OH and NO. Fluxes of these species were calculated from their ratio to sulphur in the HSC Chemistry output, and by scaling with the (prescribed) SO_2 flux in the CCATT-BRAMS model. Due to uncertainty in volcanic NO_x emissions (see discussions of Martin et al., 2012; Roberts et al., 2014a; Surl et al., 2015). Finally, HSC Chemistry output both with and without NO_x were used to initialise CCATT-BRAMS (Simulations S1_HighT and S1_HighT_noNO_x). Note that the HSC output also contains SO_3, which is the precursor to volcanic sulfate.

ACPD
15, 35313–35381, 2015

However, as mentioned above, in this study the volcanic sulfate emission was instead fixed to 1 % (by mole) of sulfur in all runs. All the emissions for the different simulations are summarized in Table 4.

Plume height

The information on plume heights is from AEROCOM database and from Bani et al. (2012). They give respectively plume heights of 1373 and of 2000 m (in our study, all the altitudes are above sea level unless otherwise mentioned). Note that the mean altitude of both crater rims is about 1000 m. Bani et al. (2012) report an altitude of the plume of 2000 m for the degassing event of 12 January 2005 that was estimated visually. For the other periods, their estimation of the altitude varies between 700 m (i.e. below the craters) and 2000 m. For the case study of the degassing event of January 2005, it was not clear to us from videos and pictures that the plume altitude was about 2000 m. As a result, we performed a sensitivity study on the plume height (see Supplement). In a first simulation, emissions are injected in the model box vertically above the volcano that includes the 1373 m altitude point. This model box is not the same in each grid, as the topography depends on the grid resolution. As a result, its depth varies between about 100–200 m. In a second simulation, emissions are injected higher up in the box containing the 2000 m altitude, whose depth varies between about 200–300 m. As shown later, we performed an additional sensitivity analysis, where the emissions are this time spread over two vertically adjacent grid boxes (Sect. 3.3.1). The depth of the plume in the model this time is about 300 to 400 m. Figure 1 shows the distribution of volcanic emissions in the vertical prescribed in the model for the different sensitivity simulations.

2.3.4 Model general set-up and simulations

In our study, the primary horizontal resolution is 50 km × 50 km with 44 vertical levels from the ground to 27 km. Three nested grids (10 km × 10 km, 2 km × 2 km and

ACPD
15, 35313–35381, 2015

0.5 km × 0.5 km) was also added. Model domain and grids are shown in Fig. 2. Horizontal winds, geopotential height, air temperature and water vapor mixing ratios from ECMWF analysis (with a 0.5° × 0.5° resolution) are used to initialize and nudge the model using a four dimensional data assimilation (4DDA) technique with a relaxation time constant ranging from 30 min at the lateral boundaries to 6 h at the center of the domain. Initial and boundary conditions for concentrations of the chemical species were provided by 6 hourly output from the global chemical transport model MOCAGE (Josse et al., 2004) with a resolution of 1° × 1°.

In the following, we describe the different simulations performed in this study. All the simulations start the 1 January 2005 00:00 UT with the larger grid only. As this was an extreme degassing event of long duration (several months) rather than an episodic eruption, the model initialization from 1 January 2005 already includes the Ambrym emissions. Due to computing limitations, the 3 nested grids are only added the 11 January 2005 00:00 UT with the initial conditions given by the corresponding simulation with one grid. The different simulations differ in terms of the strength of the emissions, the nature of the emitted compounds and the repartition of the emissions in the vertical. They are summarized below, as well as in Table 4 and Fig. 1:

- S1 includes the standard volcanic emissions (SO_2, H_2SO_4, HCl, HBr).
- S1_HighT includes emissions (SO_2, H_2SO_4, HCl, HBr, OH, NO, Cl, Br) derived from an HSC Chemistry simulation described in Sect. 2.3.3 and in Table 3.
- S0 has the same emissions as S1_HighT except that emissions from Ambrym volcano have been turned off.
- S1_HighT_alt simulation is exactly the same as S1_HighT except that the height of plume is fixed to 2000 m.
- S1_HighT_width is exactly the same than S1_HighT except that the plume of Ambrym spans two grid boxes (in the vertical) instead of one.

ACPD
15, 35313–35381, 2015

– S1_HighT_noNO$_x$ simulation is exactly the same than S1_HighT except that emissions of NO have been turned off.

– S1_nohal has the same emissions as S1_HighT except that Ambrym volcano includes only SO_2 emissions.

– S1_nohal2 has the same emissions as S1_HighT except that Ambrym volcano includes only SO_2 emissions and the same emissions of OH than S1_HighT.

– S1_HighT_surf is exactly the same than S1_HighT except area surface density was increased by a factor of 10.

In the next section, we evaluate the performances of the model CCATT-BRAMS to simulate near downwind volcanic plume chemistry for the Ambrym extreme passive degassing of 12 January 2005 in regard of the previous work and using the airborne DOAS observations of SO_2 and BrO columns.

3 Analysis of the modeled volcanic chemistry in the near downwind plume

3.1 Evaluation of the modeled SO_2 and BrO columns amounts in the near downwind plume

Figure 3 shows the SO_2 columns amounts observed during 4 traverses of the near downwind Ambrym plume (between 15 to 40 km of the vent) on 12 January 2005 between 05:00 and 06:00 UT (Bani et al., 2009, 2012) and the corresponding SO_2 columns amounts simulated by the model for the S1 (i.e. including the standard emission) and S1_HighT (i.e. initialized with the output of the HSC Chemistry model as described in Sect. 2.3.3) on the grid 0.5 km × 0.5 km (see Sect. 2.3.4 for the description of the simulations). Statistical quantities (mean, RMS, correlation) were calculated to compare more quantitatively observations and simulations (Table 5). Note that sen-

ACPD
15, 35313–35381, 2015

sitivity studies to the height of the plume and the vertical extent of the plume will be discussed further in Sect. 3.3.

3.1.1 SO_2 columns

Observations show that SO_2 columns decrease with distance from the vent and exhibit a bimodal distribution across the plume. Each mode is attributed by Bani et al. (2009) to the individual plume of the two degassing craters Benbow and Marum that are situated 3 km apart. Figure 3 shows that the model captures relatively well the magnitude of the SO_2 columns along and across the plume for the S1 and S1_HighT simulations. The mean difference between observations and simulations is lower than 2 % (relatively to the mean of the observation) and the correlation coefficient is about 0.6 (Table 5). However, we can note that the influence of the 2 craters Benbow and Marum is not seen as clearly as in the observations. This suggests a limitation linked to the model resolution, even though the model resolution for the particular grid shown is 500 m × 500 m. We can also note that the simulated plume tends to be slightly titled eastward compared to the observations in particular for the transects at 20 and 21 km (not shown) from the vent but to a lesser extent for the transect at 40 km. This is the reason for the relatively high RMS values (about 50 % of the mean SO_2, see Table 5) but it does not affect the bias (2 %).

Previous work at volcanoes elsewhere (e.g., Bobrowski et al., 2007) reported that the observed SO_2 variations in the near downwind plume are almost exclusively due to plume dilution. As a test, we have included in our simulation an SO_2 "tracer" whose emission and deposition are the same as for SO_2 but whose chemical loss is equal to zero. We find that the difference between the SO_2 columns field and the SO_2 tracer columns field at a distance of 40 km from the vent is less than 0.5 % (not shown), confirming that the SO_2 decrease in the model with distance from the vent in Fig. 3 is mostly due to plume dilution. Therefore, we can conclude from the comparison in Fig. 3 that the direction of the plume as well as its dilution are reasonably well simulated by the model in the simulations S1 and S1_HighT. It is important to note that we

ACPD
15, 35313–35381, 2015

cannot conclude here on the strength of the Ambrym SO_2 source. Indeed, our rational would be circular as we have used in our model the SO_2 source strength (described in Sect. 2.3.3 and Table 2) which Bani et al. (2009, 2012) derived from the same DOAS data (combined with winds estimates) used here for the model evaluation. Note also that we performed a simulation S1_HighT_alt, similar than S1_HighT except that the plume height was 2000 m as reported by Bani et al. (2012). We find that the simulation S1_HighT_alt (see Supplement Sect. 1 as well as Figs. S1 and S2 in the Supplement for more detail) underestimates the observations by 44 % for SO_2 (compared to 2 % for S1_HighT). The correlation between simulated and observed SO_2 is also reduced, 0.37 (compared to 0.61 for S1_HSC). Given better agreement between the model and observations at the lower injection altitude estimate of ~ 1400 m, this injection height of S1_HighT was used in the following.

3.1.2 BrO columns

In Fig. 4, the same comparison as for Fig. 3 is presented for BrO columns amounts. BrO columns, as those of SO_2, decline between 15 and 40 km from a mean of 9.8×10^{14} molecule cm^{-2} to a mean 3.2×10^{14} molecule cm^{-2}. Values as high of 1.8×10^{15} molecule cm^{-2} at 15 km were reported by Bani et al. (2009). Note that these values are particularly high compared to other BrO column observations at volcanoes elsewhere for which maximal values lie between 1×10^{14} molecule cm^{-2} to 1×10^{15} molecule cm^{-2} (Boichu et al., 2011). Note also that the influences of the two crater sources (Benbow and Marum) are still visible in the BrO data as two distinct peaks.

In the standard simulation, the trend in BrO with distance from the vent is reversed compared to the observations (also shown by the negative correlation coefficient of Table 5 of −0.21). At 15–20 km downwind from the vents where observed BrO columns are highest, the model (S1) underestimates the mean BrO columns by a factor of 10. Overall, the mean difference between BrO columns observed and those simulated in S1 is about 80 % (Table 5). An improved agreement between model and observations

ACPD
15, 35313–35381, 2015

is shown for the simulation initialized with HighT (as seen in Fig. 4): the mean bias between S1_HighT and observations is reduced and is about 40 %. In addition, the trend in BrO with distance from the crater is in better agreement with the observations (Fig. 4 and correlation coefficient of Table 5 of 0.6).

Figure 5 shows the evolution of BrO/SO_2 with distance from the vent derived from the observations and from the simulations presented in Figs. 3 and 4. Because SO_2 can be considered as a passive tracer over short timescales, any increase or decrease in BrO/SO_2 implies respectively a production or a destruction of BrO. Measurements suggest that BrO formation has occurred and has reached its maximal amount between 0 and 17 km of the vent. Further downwind, between 17 and 40 km, measurements predict a destruction of BrO. In the simulation initialized with the HSC Chemistry model, the trend in BrO/SO_2 is close to that observed. The formation of BrO reaches a maximum around 17 km with a plateau between 17 and 21 km and is destroyed between 20–21 and 40 km. In contrast, in the case of the standard simulation S1, BrO builds up between 15 and 40 km. Overall, we conclude that BrO formation is too slow in the standard simulation compared to the observations. On the contrary, the kinetics of BrO formation predicted in the simulation initialized with HSC Chemistry model is in good agreement with the observations. This confirms previous work that showed the need for radicals to "kick off" the chemistry i.e. accelerate the onset of the chemistry (e.g., Bobrowski et al., 2007; Roberts et al., 2009). In addition, Fig. 5 shows that, for each transect, the variability of BrO/SO_2 ratios in the observations and in the S1_HighT simulation have a similar magnitude. In particular, we find that for each transect the model simulates the highest value of the BrO/SO_2 ratio at the edges of the plume as shown in the observations, i.e. for lowest values of SO_2 columns. This result is again consistent with previous work (e.g., Bobrowski et al., 2007; Von Glasow, 2010; Roberts et al., 2014a). At the edges of the plume, more mixing with entrained background air occurs. This leads to higher ozone concentrations and favors BrO. In general, the trends in BrO/SO_2 with distance downwind and between core and plume edge reflect the net impact of a dynamic chemistry involving many reactive bromine chemistry species. In

ACPD
15, 35313–35381, 2015

the following section, we analyze in more detail the simulation of volcanic plume chemistry.

3.2 Simulated plume chemistry

Figure 6 shows distance-pressure cross section of SO_2, OH, HBr, BrO, O_3 and NO_x mixing ratios in the plume of the standard simulation for the 12 January 2005 at 06:00 UT (time of the DOAS measurements) in the grid 2 km × 2 km. This grid allows us to visualize the results as far as 200 km downwind. Figure 7 shows the Br speciation among the bromine species along the plume (in the core and at the edges) for the same simulation in the same grid and at the same time. Figure 6 shows that OH is totally depleted in the core of the plume in the simulation. This is due to the elevated concentrations of SO_2 as well as being a consequence of the halogen chemistry (see Sect. 4.4), and mirrors findings from previous volcano plume studies (e.g., Roberts et al., 2009, 2014a; Von Glasow, 2010). However, as noted before, the decrease of SO_2 along the plume as far as 200 km is mainly due to dilution of the plume. Figures 6 and 7 show that HBr is converted into reactive bromine in the volcanic plume, as expected. However, at about 50 km of the vent, only 20 % of this conversion had occurred (80 % HBr remains). Indeed, the chemical cycle responsible for HBr conversion is autocalytic so it needs reactive bromine to be initiated. In the standard simulation, the onset of BrO formation is slow because reactive bromine is initially formed by the reaction of HBr with OH, which is slow because OH is depleted. In Fig. 6, the enhancement of BrO (and of Br_2 in the Fig. 7) as well as the depletion of O_3, NO_x and HO_x (not shown) confirm that the autocatalytic cycle responsible for HBr conversion to reactive bromine is ongoing in the simulations. Very quickly, in the core of the plume, BrO becomes the dominant species after HBr. Its mixing ratio increases with distance from the vent reaching a maximum of 120 pptv at about 70 km (Fig. 6) equivalent to 20 % of the total bromine (Fig. 7). The depletion of ozone reaches its maximum of 15 ppbv loss (100 %) at 70 km, corresponding to the maximum of BrO. Further downwind, Br is the dominant species because O_3, HO_x and NO_x are depleted. In contrast, at the edges of

ACPD
15, 35313–35381, 2015

the plume, BrO is still increasing and dominates because more ozone is available than in the core of the plume enabling its formation from Br. Further downwind at the edges of the plume, the formation of BrO slows but does not stop (as shown by the non-zero Br_2 and BrCl fraction) as the plume disperses and dilutes the volcanic aerosol. A dynamic equilibrium is established between BrO, Br and HOBr. We can note that the BrO mixing ratio remains as high as 60 pptv at the edge of plume around 200 km downwind (Fig. 6).

As expected, in the simulation initialized with HSC Chemistry model, the conversion of HBr into reactive bromine is accelerated by the presence of the radical species (Figs. 8 and 9). Indeed, the HBr fraction is only 20 % at 25 km from the vent and is almost zero around 30 km downwind at the edge of the plume. Once HBr becomes depleted, a peak of BrCl is observed because the aqueous phase equilibria between BrCl and Br_2 favor BrCl instead of Br_2. Figure 8 shows that BrO reaches its maximum earlier, around 15–20 km downwind, than for the standard simulation (70 km), at a distance where the plume is more concentrated. As a result, the maximum of BrO mixing ratios is higher (around 240–260 pptv) than for the standard simulation. Ozone is also entirely depleted in this simulation, it reaches 15 ppbv loss (100 %) around 15 km. In the core of the downwind plume Br becomes the dominant species (up to 80 % of Bry, Fig. 9) due to this total ozone depletion with ongoing ozone loss processes exceeding any source from entrainment of (ozone-containing) background air into the plume core. HBr can reform by the reaction of Br with HCHO for instance because of the high concentrations of Br in the core of the plume. Further downwind, HBr is then slightly reconverted into BrO, likely because a somewhat enhanced entrainment of ambient air occurs. At the edges of the plume, the chemical cycles are not limited by lack of (background) oxidants. As a result, HBr can be fully consumed and BrO is the dominant species. Further downwind, the formation of reactive ongoing reactive halogen chemistry results in a dynamic equilibrium being established between BrO, Br and HOBr. To conclude, we find that the formation of reactive bromine species is faster in the S1_HighT simulation than in S1. This leads to higher BrO concentrations

ACPD
15, 35313–35381, 2015

in near downwind plume and hence to a better comparison with DOAS data. However, we can note that further downwind (approximately from 150 km of the vent), there is no significant difference between S1 and S1_HighT in terms of absolute concentration of the bromine species and in terms of partitioning among the bromine species. Despite the better comparison between DOAS and S1_HighT, the maximal BrO columns (5.7×10^{14} molecules cm^{-2}) in the S1_HighT simulation are still three times lower than the maximal values observed. We find that it is due to the ozone depletion in the core of the plume that limits the formation of BrO from Br.

In the following, we investigate the sensitivity of the model results tothe depth of the plume in the model initialization, the presence of NO_x in the emissions and the surface aerosol area density. In particular, we test whether the uncertainties in these variables could explain the discrepancies between simulations and observations.

3.3 Sensitivity studies

3.3.1 Vertical depth of the plume

A suggested in Sect. 3.2, BrO formation appears to be limited by ozone concentrations in the simulation S1_HighT. However, values of background ozone in the model seem in good agreement with ozone climatology (e.g., Logan et al., 1999) that indicates ozone mixing ratios of 15–20 ppbv below 800 hPa in the Pacific region. Here in an attempt to avoid the limitation of BrO formation due to lack of ozone, we have spread out the emissions over two vertically adjacent levels (see Fig. 1). More specifically, in the simulation S1_HighT_width, the emissions were distributed equally between the vertical grid box of the S1_HighT simulation and the one just above. In this way, the Br molecules are exposed to roughly twice as many ozone molecules. However, we find again that the comparison with DOAS SO_2 does not improve (mean bias of 17 % and a correlation of 0.55, Fig. 1s). Concerning BrO, our results are very similar to those obtained with S1_HighT (slightly worse with mean bias of 43 % and with a correlation coefficient of 0.54, Fig. 2s). This can be explained by the fact that the vertical diffusion

ACPD
15, 35313–35381, 2015

in the model has already dispersed very quickly the emissions through several vertical levels (in S1_HighT). Thus, BrO formation is already limited by ozone in the upper level where the emission was additionally injected in S1_HighT_width. However, when spreading out the emissions over more than 2 levels in the vertical, the comparison between SO_2 columns simulated and observed becomes worse (not shown) and tends to become very similar to the one obtained with S1_HighT_alt.

3.3.2 Formation of NO_x by high temperature chemistry

There are numerous uncertainties concerning the high temperature chemistry taking place in the mixture of volcanic gases and ambient air at the vent (Martin et al., 2009, 2012). In particular, models used to calculate this chemistry assume thermodynamic equilibrium. However, Martin et al. (2012) calculated that the thermal N_2 fixation is too slow for equilibrium to be attained at volcanic vents. Hence, the production of NO_x by the HSC model could be overestimated. Conversely, volcanic NO_x production is suggested by several observations of NO, NO_2, HNO_3, HO_2NO_2 in the near-source plume (e.g., Mather et al., 2004; Oppenheimer et al., 2010; Martin et al., 2012; Voigt et al., 2014), with NO_x to HNO_3 conversion pathway proposed by Roberts et al. (2009, 2014a). In the case of Ambrym, no information is available on the absence or presence of volcanic NO_x, nor other reactive nitrogen species in the plume. We performed a simulation (S1_HighT_noNO_x) where from the high-temperature initialization was not included while keeping constant the emissions of the other radicals from HSC. In this case, the SO_2 field is exactly the same as in S1_HighT (Fig. 1s). The comparison between BrO in S1_HighT_noNO_x and the observations (Fig. 2s) is very close to what is obtained for S1_HighT (mean model observation difference is about 44 % and the correlation is about 0.63). Figure 3s gives some explanation for this. It shows that the kinetics of HBr conversion in S1_HighT_noNO_x is similar to that in S1_HighT in the first 10–15 km from the vent and it is much slower after 15 km. This suggests that other radicals from the high-temperature initializationthan NO_x are crucial to kick off the chemistry initially and that afterwards NO_x emissions become important. This is

ACPD
15, 35313–35381, 2015

further confirmed by Fig. 8 when it can be seen that NO_x depletion in S1_HighT starts after 10–15 km. The role of NO_x is linked to the formation of $BrONO_2$ from BrO and NO_2 followed by its rapid hydrolysis on volcanic sulfate aerosol that acts to convert BrO into HOBr and that can then undergo another heterogeneous chemical cycle to release reactive bromine from HBr ($Br^-_{(aq)}$). Without NO_x, this conversion of BrO into HOBr can come only from reaction of BrO with HO_2. Note that due to the slower decrease of HBr in S1_HighT_noNOX after 10–15 km, no BrCl peak is visible in Fig. 3s in the near downwind in contrast to Fig. 9 for the S1_HighT simulation To conclude, the difference in BrO kinetics in S1_HighT and S1_HighT_noNO_x is mostly visible after 10–15 km from the vent. Hence, it does not impact the initial near-downwind rise in BrO. This contrasts with the model studies of Von Glasow (2010) and Surl et al. (2015) for Mt Etna who suggested a volcanic NO_x emission acts to lower plume BrO due to the formation of $BrNO_2$ that persists in the plume. However, Roberts et al. (2014a) highlighted additional pathways for $BrNO_2$ removal enabling regeneration of BrO. Given uncertainties in the chemistry, $BrNO_2$ is not included in our study.

To conclude, the simulations S1_HighT and S1_HighT_noNO_x exhibit similar kinetics of BrO formation and also a similar magnitude in the BrO maximum. As a result, uncertainty in the presence of volcanic NO_x in the emission cannot explain the discrepancy between the model and reported downwind plume BrO. In addition, we can also note that the BrO and SO_2 columns measurements alone are not sufficient to fully constrain the parameter space of our modeling of volcanic plume chemistry. In particular, NO_x and HNO_3 nitrate^{-1} should be measured in volcanic plumes to constrain the reactive nitrogen emission.

3.3.3 Sulfate aerosol surface density

In Fig. 4s, we show the simulated sulfate aerosols surface density available for heterogeneous reactions. The maximum value is 7×10^3 µm^2 cm^{-3} corresponding to a surface of 7×10^{-11} µm^2 molecule^{-1} SO_2^{-1}, a value that lies in the range of order (10^{-11}–

ACPD
15, 35313–35381, 2015

10^{-10} μm^2 molecule^{-1} SO_2) studied by Roberts et al. (2014a). It is also broadly consistent with a recent estimate of aerosol surface area (relative to SO_2) made for Mt Etna (Roberts et al., 2015). Here, we performed a sensitivity study by increasing the sulfate aerosols surface density by a factor 10 (not shown). We find that it does not impact the value of near-source BrO/SO_2 consistent with our above finding that ozone depletion is the limiting control on BrO in near-downwind Ambrym plume. This is also in agreement with the sensitivity studies performed with the PlumeChem model (Roberts et al., 2014a) for Mt Etna where increasing the aerosols surface density by a factor 10 increased only slightly the BrO/SO_2 ratio in the near downwind plume.

4 Regional impact of Ambrym volcanic emissions

4.1 Evaluation of the plume simulation at the regional scale with OMI

Figure 10 shows SO_2 columns on 12 January 2005 at 02:30 UT from OMI and the corresponding SO_2 columns interpolated on the OMI grid from CCATT-BRAMS. The model result is for the grid resolution of 10 km × 10 km that is of similar size to the OMI data (13 km × 24 km). Figure 10 suggests that the direction of the plume is correctly simulated at the regional scale. At this time of the year, the plumes from Marum and Benbow are generally carried to the northwest by the trade winds. In January 2005, they were carried to the south, because of the influence of the Cyclone Kerry, located around 1800 km southwest of Vanuatu (Bani et al., 2009). The difference between OMI and the model is mainly due to the plume width that is slightly larger in the model that in OMI (Fig. 10). In addition, further downwind in the plume some SO_2 enhancements are seen in OMI data but not in the simulations. Note that the length of the SO_2 plume in the OMI data is related to the presence of clouds north east of New Caledonia.

ACPD
15, 35313–35381, 2015

4.2 Impact of Ambrym on sulfate, bromine and ozone at the regional scale

Our simulations include 4 grids. To study impacts of Ambrym at the regional scale, model outputs for the largest grid (see Fig. 2), whose resolution is 50 km × 50 km, are analyzed. Because of computing limitations, we present only the impact for the 12 January 2005 after 11 days of spin-up.

4.2.1 Sulfate

The sulfate burden in the model domain due to Ambrym increases by 44 % (i.e. 0.08 Tg of sulfate), value calculated as the mean difference in sulfate between S1_HighT and S0 for 12 January. The direct sulfate emission totals 3.34 Gg of sulfate since the beginning of the simulation. This means that at least 96 % of the sulfate burden increase due to Ambrym results from the atmospheric oxidation of SO_2 from the volcano by OH. It is a lower limit as direct emissions could have left the domain during the simulation or have undergone deposition. Thus we confirm that sulfate formed from atmospheric oxidation of SO_2 is the dominant driver of the plume halogen chemistry on the regional scale. This contrasts to the near-downwind plume where the directly emitted sulfate (formed from high-temperature SO_3) is dominant and is essential for the rapid formation of BrO (see Roberts et al., 2009; von Glasow, 2010). Figure 11 shows the spatial distribution of sulfate due to Ambrym emissions calculated as the daily mean difference between the simulation S1_HighT and S0 for 12 January 2005. The vertical profile of this daily averaged (across the domain) sulfate is also shown in Fig. 12 for S1_HighT and S0 simulations. This Figure shows that the contribution of Ambrym to the sulfate in the domain is mostly confined below 600 hPa. The Fig. 11 indicates that it can reach 2.5 ppbv in the plume at 875 hPa, the approximate altitude of the emissions injection in the simulation. The contribution of Ambrym is also particularly high (hundreds of pptv) in an extensive zone west of the volcano at 875 hPa. In the middle troposphere (500 hPa) and in the Tropical Tropopause Layer (150 hPa), the influence of Ambrym is more localized. It is co-localized with convective events as can be seen in the precipi-

ACPD
15, 35313–35381, 2015

tation data of the TRMM (Tropical Rainfall Measuring Mission) satellite (Huffman et al., 2007) and simulated by the model (Fig. 13). More precisely, the 500 hPa enhancement is co-localized with a band of convective systems situated south east of New Caledonia the 12 and the days prior. This is further confirmed by the analysis of forward trajectories initialized from Ambrym on the 10 and the 11 January 2005 (Fig. 14) calculated with the HYSPLIT transport and dispersion model (Draxler and Rolph, 2003). The enhancement of sulfate at 150 hPa is co-localized with a convective event that happened north of Vanuatu the 11 as suggested by the TRMM data (not shown) and could also be resulting from transport from a convective event that occurred south as shown in Fig. 13. These localized enhancements of sulfate in the middle and upper troposphere due to Ambrym can reach 700 pptv at 500 hPa and 250 pptv at 150 hPa. Overall, over the whole domain, above 600 hPa, the influence of Ambrym emissions is reduced: sulfate mixing ratios are increased by 30 pptv for example at 300 hPa. This is explained by the fact that sulfate is strongly washed-out by precipitation in the model. In this model study, the aqueous-phase oxidation of SO_2 to sulfate was not taken into account. This process becomes self-limiting in strong volcanic plumes due to the titration of oxidants for example H_2O_2 (Schmidt et al., 2010) but may have a significant contribution to sulfate formation over the whole model domain thus will be considered in future work.

4.2.2 Bromine

Figure 15 shows the horizontal distribution of the total bromine content ($Bry = HBr + 2Br_2 + BrCl + Br + BrO + HOBr + BrONO_2$) due to Ambrym emissions calculated as the daily mean difference between the simulation S1_HighTand S0 for 12 January 2005. The vertical profile of this daily averaged Bry is shown in Fig. 16 for S1_HighT and S0 simulations. The results presented here are for the larger grid whose resolution is 50 km × 50 km. The regional influence of Ambrym volcano emissions as a source of Bry is clearly demonstrated. Ambrym is the main volcanic source of bromine in the domain, causing a regional plume of enhanced Bry (maximum of 60 pptv) in the lower troposphere. Bagana volcano in Papua New Guinea was also ac-

ACPD
15, 35313–35381, 2015

tive at this time (see Sect. 2.3.3), and is responsible for a smaller enhancement in the S0 simulation around 875 hPa seen in Fig. 16. In the middle troposphere (500 hPa) and in the Tropical Tropopause Layer (150 hPa), the influence of Ambrym is still visible but more localized, increasing locally the background Bry by up to 3 pptv. The same convective events as those mentioned in the previous section are responsible for these Bry enhancements. There is also evidence of transport to the stratosphere when analysing results at 80 hPa (a model level that is above the thermal tropopause in the simulation) with a few visible patches of Bry of up to 0.5 pptv. Such transport of volcanic bromine to the upper troposphere and the stratosphere is of strong interest. Indeed, the stratospheric bromine burden is underestimated by global models that take only into account long lived halons and methyl bromide. The missing source is believed to arise from bromine containing very short lived substance (VSLS) (i.e. bromocarbon source gases whose lifetime is less than 6 months, their degradation products as well as inorganic sources of bromine in the troposphere) transported from the boundary layer to the stratosphere. Their contribution to the stratospheric bromine loading ranges between 2–8 pptv (Carpenter et al., 2014). Here, we find that bromine emissions from Ambrym are responsible for a mean increase of 0.3 pptv of Bry in the model domain at the altitude of the plume (875 hPa), and of 0.1 pptv around 300 hPa in the upper troposphere (Fig. 16). Locally enhancements of 3 pptv are simulated in the upper troposphere due to convective transport and there is also evidence of transport to the stratosphere (up to 80 hPa) of Bry from Ambrym as mentioned above. Figure 16 also presents the vertical profile of daily mean Br^- speciation of volcanic Bry. We have only considered the model grid boxes strongly influenced by volcanic bromine (for which the mean difference between S1_HighTand S0 was higher than 0.5 pptv in Fig. 15). It is clear from this figure that the partitioning strongly varies with altitude. In the lower troposphere, as seen previously at the local scale in Sect. 3.2, HBr is readily depleted by its conversion into reactive bromine by the reaction of HOBr on sulfate aerosol, that produces Br_2 and/or BrCl. BrCl dominates which is surprising as it is readily photolysed, and was not found to be a major component of reactive bromine at the local plume-scale (Sect. 3.2).

ACPD
15, 35313–35381, 2015

This is most likely due to very rapid halogen cycling on sulfate aerosol, whose concentration increases as more volcanic SO_2 is oxidized in the downwind plume. HOBr also contributes to a significant fraction of Bry at the regional scale at 875 hPa consistent with its role of reservoir of reactive bromine when the plume becomes diluted. The greater influence of photolysis reactions at higher altitudes is shown in the profiles by the declining HOBr and increasing Br with altitude that causes BrO also to increase. HOBr can also be washed out by precipitation. There is a back-conversion of reactive bromine species (Br and BrO) into HBr at higher altitude above 300 hPa. It is caused by reaction of volcanic Br with HO_2. Note that the difference between Bry from S1 and from S1_HighT (not shown) is small and can reach a maximum of 3 pptv in regions of Ambrym plume that reach up to 60 pptv Br_y at 875 hPa.

4.2.3 Ozone

Figure 17 shows the variation of ozone due to Ambrym emissions calculated as the daily mean difference in percent (of S0) between the simulation S1_HighT and S0 for 12 January 2005. The magnitude of ozone depletion in the simulation S1_HighT is correlated with the change of sulfate and of bromine due to Ambrym emissions (Figs. 11 and 15). At 875 hPa, it is maximal (40 %) in the concentrated plume and significant (> 10 %) in an extensive zone west of the volcano strongly influenced by Ambrym emissions (Figs. 11 and 15). Note that during the day, the depletion can be total in the plume (not shown) as presented at plume scale (Fig. 8). Transport of an ozone depleted air mass by convection can also be seen at 500 hPa. At higher altitudes, the influence of Ambrym on ozone mixing ratios is smaller, less than 2 %. When the whole domain is considered, Ambrym emissions are responsible for an ozone depletion of 72 Gg in the S1_HighT simulation, it represents 0.2 % of the ozone content in the domain (32 Tg of ozone). In the S1 simulation, depletion of ozone due to Ambrym totals 69 Gg of ozone. It is consistent with the fact that high temperature chemistry is only important in approximately the first 150 km from the source in our simulation as shown in Sect. 3.2.

ACPD
15, 35313–35381, 2015

4.3 Impact of Ambrym emissions on the oxidizing power of the troposphere

The oxidizing capacity of the troposphere determines the atmospheric fate of many atmospheric pollutants including greenhouse gases such as methane, thus is an important control on tropospheric composition and climate. Volcanic emissions are expected to impact the oxidizing power of the atmosphere in several ways. First, the large amounts of SO_2 emitted by volcanoes react with OH, drastically reducing its concentration. Furthermore, the conversion of emitted halogen halides to more reactive halogen species in volcanic plumes results in chemical cycles that deplete ozone and HO_2 (and therefore OH), as well as NO_x that can in turn also affect ozone and OH. In addition, these reactive halogen cycles produce chlorine radicals that can also oxidize methane and non-methane hydrocarbons. Here, to illustrate the impact of Ambrym during the extreme degassing event of January 2005 on the oxidizing capacity of the atmosphere, we calculate change to the lifetime of a key atmospheric greenhouse gaz: methane. In particular, we investigate the relative contribution of the different components of the volcanic emissions to the overall perturbation of methane lifetime due to Ambrym degassing.

Methane is a key greenhouse gas with both natural and anthropogenic sources, whose main loss pathway from the atmosphere is by gas-phase reaction with OH. Methane lifetime due to a process (e.g., reaction with OH) is commonly defined as the total methane atmospheric burden (Tg) at steady state (i.e. with unchanged burden) divided by total methane losses through this process ($\mathrm{Tg\,yr^{-1}}$) (IPCC, 2001). We have applied this definition here. However, it is important to highlight that to calculate a proper methane lifetime we would have to perform a simulation of about 10 years with a global model. Instead, we have calculated the instantaneous perturbation of CH_4 lifetime over the model domain (averaged over a day), which reflects the instantaneous perturbation of the methane sink on a regional scale. The results in terms of lifetime change cannot be extrapolated to the global scale and depend also strongly on the area of the model domain. Our aim here is to assess the relative contribution of volcanic sul-

ACPD
15, 35313–35381, 2015

fur emissions and reactive halogen plume chemistry on the overall perturbation of CH_4 lifetime.

We calculate that the methane lifetime due to reaction of methane with OH, τ_{CH_4+OH}, is about 4.65 years in our simulation when the volcanic emission from Ambrym is not included. A value of 9.7 ± 1.5 yr is derived from most recent studies based on global modeling (Naik et al., 2012). The shorter methane lifetime calculated here reflects the condition in the tropics for January where the OH concentration is particularly high. We find that τ_{CH_4+OH} increases by 0.97 % due to volcanic emissions in the simulation S1_HighT compared to the simulation S0. For the simulation with volcanic SO_2 emissions alone (S1_nohal), we calculate that the methane lifetime τ_{CH_4+OH} increase is only about 0.37 %. Therefore we infer that about 62 % of the increase of τ_{CH_4+OH} due to volcanic emissions is due to halogen chemistry cycles that deplete HO_x and ozone.

A second consideration is that the volcano plume chlorine can itself react with methane, decreasing its lifetime. The methane lifetime due to reaction with Cl, τ_{CH_4+Cl} is 246 years in our simulation without volcanic emission from Ambrym (S0). This compares well to the methane lifetime of about 200 years derived by Allan et al. (2007). When Ambrym emissions are included, τ_{CH_4+Cl} decreases by 17 % to 204 years due to reaction with reactive chlorine produced in Ambrym plume. Nevertheless, this reduction in methane lifetime due to Cl radicals only partially counters the increase in methane lifetime caused by the decrease of OH (through both volcanic plume halogen cycles and SO_2). The net volcanic impact is an overall 0.57 % increase in methane lifetime. Thus, the effect of chlorine radicals on the methane lifetime counteracts 41 % of the effect due to the OH decrease. Note that very recent measurements of reactive chlorine (OClO) in Mt Etna volcanic plume (General et al., 2014; Gliß et al., 2015) could help to better quantify the impact of chlorine radicals on the methane lifetime.

4.4 Impact of Ambrym emissions on SO_2 lifetime

As already discussed in the Introduction, SO_2 undergoes atmospheric oxidation into sulfate aerosols that exert climatic impacts from both direct radiative and indirect

ACPD
15, 35313–35381, 2015

cloud albedo effects (Schmidt et al., 2012). Sinks of SO_2 are dry and wet deposition, gas phase oxidation and aqueous phase oxidation. The estimated lifetime of SO_2 in the troposphere by global models ranges between 0.6–2.6 days (e.g., Rotstayn and Lohmann, 2002 and references therein), with a lifetime with respect to gas-phase oxidation by OH of around 2 weeks (e.g., Rotstayn and Lohmann, 2002; Von Glasow, 2009). However, model studies indicate a lengthened lifetime for volcanic SO_2 (e.g., Chin and Jacob, 1996; Graf et al., 1997; Stevenson et al., 2003; Schmidt et al., 2010). For example, a lifetime of 24–34 days was calculated for the Laki 1783-4 eruption using a global model (Schmidt et al., 2010). This is due to volcanic plume injection into the free troposphere (where removal rates are much lower than in the boundary layer) and suppression of oxidants (OH, H_2O_2, noting limited role of ozone under acid conditions) by the SO_2 chemistry. Our regional 3-D model study includes a less detailed SO_2-sulfate chemistry scheme (gas-phase oxidation only) but includes detailed plume reactive halogen chemistry. Here, we have calculated the impact of volcanic halogen chemistry on the lifetime of SO_2 due to gas phase oxidation by OH. More precisely, we calculate the lifetime of SO_2 in the whole domain and of SO_2 in the plume from Ambrym (defined in our study as model grids where $SO_2 > 5$ ppbv). For the simulation S1_nohal (that includes only SO_2 emissions) and for the whole domain of the simulation, we find a lifetime of SO_2 of 8.8 days consistent with previous work given that the simulation is for the tropics. For this S1_nohal simulation and considering only the plume of Ambrym, the lifetime of SO_2 increases (11 days). This is consistent with the known self-limitation of SO_2 oxidation in volcanic plumes as OH becomes depleted in the plume by the reaction with SO_2 itself. For the simulation including volcanic halogens with high-temperature initialization, S1_HighT, the SO_2 lifetime for the whole domain is 8 days and for the plume 5.5 days. This result of shorter SO_2 lifetime in the plume than in the whole domain is initially surprising because of the self-limitation of SO_2 oxidation as explained above. The shorter SO_2 lifetimes for S1_HighTcompared to S1_nohal are also again surprising because the halogen chemistry acts to further deplete OH in the plume. These results are explained by the OH emissions in S1_HighT

ACPD
15, 35313–35381, 2015

(high-temperature initialization) that provides an additional rapid near-source sink for SO_2, thereby contributing to the effective volcanic sulfate emission. This is confirmed by the simulation, S1_nohal2 (that includes SO_2 emissions and OH emissions from HSC chemistry but no halogens), in which the SO_2 lifetimes are 7.5 days for whole domain and 5.6 days for the plume. This impact of high-temperature OH source on volcanic SO_2 occurs very close to source (after which OH becomes depleted), leading to an unexpected shortening of the calculated SO_2 lifetime, that complicates the lifetime calculation. A similar effect was not seen for methane because it is not co-emitted from the volcano and OH is preferentially titrated by SO_2 (and HCl).

Because of the complication of the lifetime calculation in S1_HighT, it is better to compare the simulations with (S1) and without (S1_nohal) halogen emissions, excluding high-temperature chemistry. We have shown before that simulations with and without high temperature chemistry give very similar results in terms of Bry and ozone at the regional scale (see Sect. 4.2.2 and 4.2.3). In the simulation S1, the SO_2 lifetime is 15 days in the plume and 9.4 days for the whole domain. This results is consistent with what it is expected as the lifetime of SO_2 is lengthened in the plume compared to the S1_nohal (SO_2 emission only) simulation (11 days). We conclude that volcanic halogen chemistry increases the lifetime of SO_2 in the plume by 36 % through its impact on OH. Similarly, SO_2 lifetime is also increased by halogen chemistry for the whole domain, but by a lesser extent (9.4 days compared to 8.8 days in S1_nohal).

5 Conclusions

The CCATT-BRAMS meso-scale model was used and further developed to study the impact of Ambrym volcano emissions, Vanuatu (Southwest Pacific), on the chemical composition of the atmosphere at the local and regional scales. We focus on an episode of extreme passive degassing of Ambrym that lasted several months in early 2005, and for which SO_2 and BrO columns airborne DOAS measurements in the plume have been reported. Model development includes the incorporation of reactive halo-

ACPD
15, 35313–35381, 2015

gen chemistry and a volcano emission source specific to Ambrym. Using the nesting grid capability of CCATT-BRAMS, we simulate the Ambrym plume at high resolution (500 m × 500 m). This allows us to make a direct (unbiased) comparison with DOAS SO_2 and BrO data, and hence test our understanding of volcanic plume chemistry at the plume level. We find that the model reproduces reasonably well the spatial distribution of SO_2 in the near downwind plume (i.e. the direction and dilution of the plume). The model captures the salient features of volcanic chemistry as reported in previous work such as HO_x and ozone depletion in the core of the plume. With the simulation initialized with high temperature chemistry at the vent (that produces: Br, Cl, HO_x and NO_x radical species), the pattern of BrO/SO_2 trend with distance downwind and across the plume simulated by the model is in good agreement with the DOAS observations. However, the magnitude of the maximal BrO enhancement in the plume is underestimated by the model by a factor 3. The analysis of the model results shows that BrO formation is ozone limited in the near-downwind plume due to the combination of a low background ozone (15 ppbv, of which 100 % is depleted in the plume) and the high emissions flux from Ambrym.

This study confirms the importance of the high temperature chemistry at the vent to reproduce BrO/SO_2 variation in the near downwind plume. It also demonstrates that the (non-sulfur) radicals produced by the high temperature chemistry are mostly important for the initial rise of BrO/SO_2 at Ambrym. Further downwind from the vents (after 150 km approximately for our case), simulations with and without the high-temperature initialization exhibit rather similar chemistry. Nevertheless, the primary aerosol emission, that is crucial to enable the heterogeneous chemistry producing reactive bromine in the near downwind plume, originates from the high-temperature plume chemistry at the vent. It was kept constant in these simulations (at 1 % of total sulfur) and hence its impact is not taken into account when comparing simulations with and without high temperature chemistry.

Impacts of Ambrym in Southwest Pacific region were also evaluated across the larger model grid domain. In the lower troposphere, at altitudes close to the injection height

ACPD
15, 35313–35381, 2015

(875 hPa), Ambrym causes a substantial increase in sulfate (from 0.1 to 2.5 ppbv) and in bromine mixing ratios (from 0.1 to 60 pptv). Transport of bromine species (as well as sulfate) to the upper troposphere due to convection is also predicted by the model, with convective regions confirmed by the precipitation data from the TRMM satellite as well as by trajectories from the HYSPLIT transport and dispersion model. There is also evidence in the simulations of a subsequent transport of bromine to the stratosphere from Ambrym. In future work, longer duration simulations should be performed to fully quantify the impact of Ambrym on chemical composition of the troposphere at the regional scale. In particular, flux of bromine to upper troposphere and to the stratosphere from this extreme continuous degassing event, as well as during the typical continuous emission from Ambrym should be calculated. This will provide insight to the importance of Ambrym volcano plume to the budget and chemistry of bromine in these regions. Ozone depletion (between 5 to 40 %) is ongoing albeit slower in the extensive region few thousands of kilometres from the volcano influenced by the dispersed plume. We find a tropospheric ozone depletion of 72 Gg, (i.e.: 0.2 % for a domain containing 32 Tg of ozone) in the model domain.

This influence of the plume chemistry on tropospheric oxidants (depletion of HO_x and ozone by reactive halogen chemistry and depletion of OH by oxidation of SO_2) in turn affects other atmospheric species in the model. We show that methane lifetime (with respect to its reaction with OH and with Cl) in the model is increased when volcanic emissions are taken into account, confirming the potential for volcanic emissions to influence the oxidizing power of the atmosphere. Furthermore, we find that reactive halogen chemistry is responsible for more than half of the perturbation (62 %) of methane lifetime with respect to OH, with depletion of OH by SO_2 chemistry responsible for the remainder. Cl radicals produced in the plume counteract some of the effect (41 %) of the methane lifetime lengthening due to OH depletion. This work thereby particularly highlights the impact of reactive volcanic halogen chemistry on the oxidizing capacity of the atmosphere. Here, it is found to be more important than the impact of OH depletion by volcanic SO_2. However, the reactive halogen mediated HO_x depletion

ACPD
15, 35313–35381, 2015

and Cl radical formation exert opposing impacts on the methane lifetime. Furthermore, we calculate an increase of 36 % in the SO_2 lifetime with respect to oxidation by OH due to reactive halogen chemistry in the plume that depletes HO_x and ozone. Thus reactive halogen chemistry exerts a significant influence on the volcanic SO_2 lifetime hence also on the production of sulfate. This needs to be taken into account in studies evaluating the impact of volcanoes on radiative forcing. Especially if the injection height is high in altitude, the sink of SO_2 by OH can be the dominant oxidation pathway and thus exert a major control on SO_2 lifetime and sulfate formation (Schmidt et al., 2010). Uncertainties in the modelled plume chemistry include aspects of the volcanic emissions, and also the rate of heterogeneous reaction of HOBr on the volcanic aerosol, which is a key driver of the reactive halogen cycling hence the plume regional impacts. This depends on the aerosol surface area and underlying chemical kinetics (for which a re-evaluation for acidic plume conditions was made by Roberts et al., 2014b). Ongoing work is aimed at improving the aerosol and HOBr reactive uptake parameterization in the model. Transects across the plume at various distances from the vents, as performed by Bani et al. (2009), appear very useful altogether with a model to test our understanding of the dynamics of volcanic plume chemistry. Nevertheless, this study emphasizes the need to measure more chemical species to constrain knowledge of the volcanic plume chemistry as also highlighted in Brobowski et al. (2015). In particular, the coupling between BrO_x (= Br + BrO) and NO_x appears rather uncertain (Roberts et al., 2014a). Measurements of BrO and SO_2 are not sufficient to fully constrain the plume chemistry; background ozone as well as in plume ozone, HO_x, NO_x, as well as other bromine compounds than BrO and size-resolved aerosol characterisation are needed along with a better characterisation of the plume injection height and of the plume depth (width in general being constrained by satellite and DOAS transects). To be most insightful, studies should combine the systematic downwind plume investigation with (simultaneous) detailed crater-rim measurements to constrain the volcanic gas and aerosol emission. Recent advances in satellite detection of reactive halogen

ACPD
15, 35313–35381, 2015

species in tropospheric volcanic plumes (Hörmann et al., 2013) may also be used in future regional and global model studies of volcanic activity impacts.

The Supplement related to this article is available online at doi:10.5194/acpd-15-35313-2015-supplement.

Acknowledgements. This work was supported by the LABEX VOLTAIRE (VOLatils – Terre Atmosphère Interactions – Ressources et Environnement) ANR-10-LABX-100-01 (2011-20). The authors benefitted from the use of the cluster at the Centre de Calcul Scientifique en région Centre. We gratefully acknowledge Saulo Freitas (NOAA/ESRL/CPTEC) for his help with the CCATT-BRAMS model and Laurent Catherine (OSUC) for technical help with the cluster at Centre de Calcul Scientifique en région Centre. We thank P. Bani (IRD) and C. Oppenheimer (University of Cambridge) for providing their DOAS data, Virginie Marécal (CNRM/Météo-France) for initiating the project and Bruno Scaillet (ISTO) for providing some earlier HCl/SO_2 and HBr/SO_2 ratios.

We are grateful to the NOAA Air Resources Laboratory for the provision of the HYSPLIT Transport and dispersion model (http://www.arl.noaa.gov/ready/hyslit4.html).

References

Aiuppa, A., Federico, C., Franco, A., Giudice, G., Gurrieri, S., Inguaggiato, S., Liuzzo, M., McGonigle, A. J. S., and Valenza, M.: Emission of bromine and iodine from Mount Etna volcano, Geochem. Geophy. Geosy., 6, Q08008, doi:10.1029/2005GC000965, 2005.

Allan, W., Struthers, H., and Lowe, D. C.: Methane carbon isotope effects caused by atomic chlorine in the marine boundary layer: global model results compared with Southern Hemisphere measurements, J. Geophys. Res., 112, D04306, doi:10.1029/2006JD007369, 2007.

Allard, P., Aiuppa, A., Bani, P., Metrich, N., Bertagnini, A., Gauthier, P. J., Parelli, F., Sawyer, G. M., Shinohara, H., Bagnator, E., Mariet, C., Garebiti, E., and Pelletier, B.: Ambrym basaltic volcano (Vanuatu Arc): volatile fluxes, magma degassing rate and chamber depth, in: AGU Fall Meeting Abstracts, Vol. 1, San Francisco, USA, December 2009.

Allard, P., Aiuppa, A., Bani, P., Métrich, N., Bertagnini, A., Gauthier, P. J., Shinohara, H., Sawyer, G., Parello, F., Bagnato, E., and Pelletier, B.: Prodigious emission rates and magma degassing budget of major, trace and radioactive volatile species from Ambrym basaltic volcano, Vanuatu island Arc, J. Volcanol. Geoth. Res., doi:10.1016/j.jvolgeores.2015.10.004, online first, 2015.

Allibone, R., Cronin, S. J., Douglas, C. T., Oppenheimer, C., Neall, V. E., and Stewart, R. B.: Dental fluorosis linked to degassing on Ambrym volcano, Vanuatu: a novel exposure, pathway, Environ. Geochem. Hlth., 34, 155–170, doi:10.1007/s10653-010-9338-2, 2010.

Andres, R. J. and Kasgnoc, A. D.: A time-averaged inventory of subaerial volcanic sulfur emissions, J. Geophys. Res.-Atmos., 103, 25251–25261, 1998.

Arteta, J., Marécal, V., and Rivière, E. D.: Regional modelling of tracer transport by tropical convection – Part 1: Sensitivity to convection parameterization, Atmos. Chem. Phys., 9, 7081–7100, doi:10.5194/acp-9-7081-2009, 2009a.

Arteta, J., Marécal, V., and Rivière, E. D.: Regional modelling of tracer transport by tropical convection – Part 2: Sensitivity to model resolutions, Atmos. Chem. Phys., 9, 7101–7114, doi:10.5194/acp-9-7101-2009, 2009b.

Atkinson, R., Baulch, D. L., Cox, R. A., Crowley, J. N., Hampson, R. F., Hynes, R. G., Jenkin, M. E., Rossi, M. J., and Troe, J.: Evaluated kinetic and photochemical data for atmospheric chemistry: Volume III – gas phase reactions of inorganic halogens, Atmos. Chem. Phys., 7, 981–1191, doi:10.5194/acp-7-981-2007, 2007.

Bani, P., Oppenheimer, C., Tsanev, V. I., Carn, S. A., Cronin, S. J., Crimp, R., Calkins, J. A., Charley, D., Lardy, M., and Roberts, T. R.: Surge in sulphur and halogen degassing from Ambrym volcano, Vanuatu, B. Volcanol., 71, 1159–1168, 2009.

Bani, P., Oppenheimer, C., Allard, P., Shinohara, H., Tsanev, V., Carn, S., Lardy, M., and Garaebiti, E.: First estimate of volcanic SO_2 budget for Vanuatu Isl. Arc, J. Volcanol. Geoth. Res., 211, 36–46, 2012.

Barrie, L. A., Bottenheim, J. W., Schnell, R. C., Crutzen, P. J., and Rasmussen, R. A.: Ozone Destruction and Photochemical Reactions at Polar Sunrise in the Lower Arctic Atmosphere, Nature 334, 138–141, doi:10.1038/334138a0, 1988.

Bela, M. M., Longo, K. M., Freitas, S. R., Moreira, D. S., Beck, V., Wofsy, S. C., Gerbig, C., Wiedemann, K., Andreae, M. O., and Artaxo, P.: Ozone production and transport over the Amazon Basin during the dry-to-wet and wet-to-dry transition seasons, Atmos. Chem. Phys., 15, 757–782, doi:10.5194/acp-15-757-2015, 2015.

ACPD
15, 35313–35381, 2015

Bhartia, P. K. and Wellemeyer, C. W.: OMI TOMS-V8 Total O_3 Algorithm, Algorithm Theoretical Baseline Document: OMI Ozone Products, edited by: Bhartia, P. K., Vol. II, ATBD-OMI-02, version 2.0, available at: http://eospso.gsfc.nasa.gov/sites/default/files/atbd/ATBDOMI-02.pdf (last access: November 2015), 2002.

Bobrowski, N. and Platt, U.: SO_2 BrO^{-1} ratios studied in five volcanic plumes, J. Volcanol. Geoth. Res., 166, 3, 147–160, 2007.

Bobrowski, N., Hönninger, G., Galle, B., and Platt, U.: Detection of bromine monoxide in a volcanic plume, Nature, 423, 273–276, 2003.

Bobrowski, N., Von Glasow, R., Aiuppa, A., Inguaggiato, S., Louban, I., Ibrahim, O. W., and Platt, U.: Reactive halogen chemistry in volcanic plumes, J. Geophys. Res.-Atmos., 112, D06311, doi:10.1029/2006JD007206, 2007.

Bobrowski, N., Glasow, R., Giuffrida, G. B., Tedesco, D., Aiuppa, A., Yalire, M., Arellano, S., Johansson, M., and Galle, B.: Gas emission strength and evolution of the molar ratio of BrO/SO_2 in the plume of Nyiragongo in comparison to Etna, J. Geophys. Res.-Atmos., 120, 277–291, 2015.

Boichu, M., Oppenheimer, C., Roberts, T. J., Tsanev, V., and Kyle, P. R.: On bromine, nitrogen oxides and ozone depletion in the tropospheric plume of Erebus volcano (Antarctica), Atmos. Environ., 45, 3856–3866, 2011.

Carpenter, L. J., Reimann, S., Burkholder, J. B., Clerbaux, C., Hall, B. D., Hossaini, R., Laube, J. C., and Yvon-Lewis, S. A.: Ozone-Depleting Substances (ODSs) and other gases of interest to the Montreal protocol, chapter 1, in: Scientific Assessment of Ozone Depletion: 2014, Global Ozone Research and Monitoring Project – Report No. 55, World Meteorological Organization, Geneva, Switzerland, 2014.

Carslaw, K. S., Lee, L. A., Reddington, C. L., Pringle, K. J., Rap, A., Forster, P. M., Mann, G. W., Spracklen, D. V., Woodhouse, M. T., Regayre, L. A., and Pierce, J. R.: Large contribution of natural aerosols to uncertainty in indirect forcing, Nature, 503, 67–71, 2013.

Chin, M. and Jacob, D. J.: Anthropogenic and natural contributions to tropospheric sulfate: a global model analysis, J. Geophys. Res.-Atmos., 101, 18691–18699, 1996.

Delmelle, P.: Environmental impacts of tropospheric volcanic gas plumes, Geol. Soc. Spec. Publ., 213, 381–400, 2003.

Diehl, T., Heil, A., Chin, M., Pan, X., Streets, D., Schultz, M., and Kinne, S.: Anthropogenic, biomass burning, and volcanic emissions of black carbon, organic carbon, and SO_2 from

ACPD
15, 35313–35381, 2015

1980 to 2010 for hindcast model experiments, Atmos. Chem. Phys. Discuss., 12, 24895–24954, doi:10.5194/acpd-12-24895-2012, 2012.
Draxler, R. R. and Rolph, G. D.: HYSPLIT (HYbrid Single-Particle Lagrangian Integrated Trajectory) Model access via NOAA ARL READY Website, available at: http://ready.arl.noaa.gov/HYSPLIT.php, last access: November 2015.
Fan, S.-M. and Jacob, D. J.: Surface ozone depletion in Arctic spring sustained by bromine reactions on aerosols, Nature, 359, 522–524, 1992.
Freitas, S. R., Longo, K. M., Silva Dias, M. A. F., Chatfield, R., Silva Dias, P., Artaxo, P., Andreae, M. O., Grell, G., Rodrigues, L. F., Fazenda, A., and Panetta, J.: The Coupled Aerosol and Tracer Transport model to the Brazilian developments on the Regional Atmospheric Modeling System (CATT-BRAMS) – Part 1: Model description and evaluation, Atmos. Chem. Phys., 9, 2843–2861, doi:10.5194/acp-9-2843-2009, 2009.
Freitas, S. R., Longo, K. M., Alonso, M. F., Pirre, M., Marecal, V., Grell, G., Stockler, R., Mello, R. F., and Sánchez Gácita, M.: PREP-CHEM-SRC – 1.0: a preprocessor of trace gas and aerosol emission fields for regional and global atmospheric chemistry models, Geosci. Model Dev., 4, 419–433, doi:10.5194/gmd-4-419-2011, 2011.
General, S., Bobrowski, N., Pöhler D., Weber, K., Fischer, C., and Platt, U.: Airborne I-DOAS measurements at Mt. Etna: BrO and OClO evolution in the plume, J. Volcanol. Geoth. Res., 300, 175–186, doi:10.1016/j.jvolgeores.2014.05.012, 2014.
Gerlach, T. M.: Volcanic sources of tropospheric ozone-depleting trace gases, Geochem. Geophy. Geosy., 5, Q09007, doi:10.1029/2004GC000747, 2004.
Gliß, J., Bobrowski, N., Vogel, L., Pöhler, D., and Platt, U.: OClO and BrO observations in the volcanic plume of Mt. Etna – implications on the chemistry of chlorine and bromine species in volcanic plumes, Atmos. Chem. Phys., 15, 5659–5681, doi:10.5194/acp-15-5659-2015, 2015.
Graf, H. F., Feichter, J., and Langmann, B.: Volcanic sulfur emissions: estimates of source strength and its contribution to the global sulfate distribution, J. Geophys. Res.-Atmos., 102, 10727–10738, 1997.
Grellier, L., Marécal, V., Josse, B., Hamer, P. D., Roberts, T. J., Aiuppa, A., and Pirre, M.: Towards a representation of halogen chemistry within volcanic plumes in a chemistry transport model, Geosci. Model Dev. Discuss., 7, 2581–2650, doi:10.5194/gmdd-7-2581-2014, 2014.
Guenther, A., Karl, T., Harley, P., Wiedinmyer, C., Palmer, P. I., and Geron, C.: Estimates of global terrestrial isoprene emissions using MEGAN (Model of Emissions of Gases and

ACPD
15, 35313–35381, 2015

Aerosols from Nature), Atmos. Chem. Phys., 6, 3181–3210, doi:10.5194/acp-6-3181-2006, 2006.
Halmer, M. M., Schmincke H- U., and Graf, H.-F.: The annual volcanic gas input into the atmosphere, in particular into the stratosphere: a global data set for the past 100 years, J. Volcanol. Geoth. Res., 115, 511–528, 2002.
Hebestreit, K., Stutz, J., Rosen, D., Matveiv, V., Peleg, M., Luria, M., and Platt, U.: DOAS measurements of tropospheric bromine oxide in mid-latitudes, Science, 283, 55–57, 1999.
Hörmann, C., Sihler, H., Bobrowski, N., Beirle, S., Penning de Vries, M., Platt, U., and Wagner, T.: Systematic investigation of bromine monoxide in volcanic plumes from space by using the GOME-2 instrument, Atmos. Chem. Phys., 13, 4749–4781, doi:10.5194/acp-13-4749-2013, 2013.
Huffman, G. J., Adler, R. F., Bolvin, D. T., Gu, G., Nelkin, E. J., Bowman, K. P., Hong, Y., Stocker, E. F., and Wolff, D. B.: The TRMM multi-satellite precipitation analysis: quasi-global, multi-year, combined-sensor precipitation estimates at fine scale, J. Hydrometeorol., 8, 38–55, 2007.
Josse, B., Simon, P., and Peuch, V.-H.: Radon global simulations with the multiscale chemistry and transport model MOCAGE, Tellus B, 56, 339–356, 2004.
Kelly, P. J., Kern, C., Roberts, T. J., Lopez, T., Werner, C., and Aiuppa, A.: Rapid chemical evolution of tropospheric volcanic emissions from Redoubt Volcano, Alaska, based on observations of ozone and halogen-containing gases, J. Volcanol. Geoth. Res., 259, 317–333, 2013.
Kern, C., Sihler, H., Vogel, L., Rivera, C., Herrera, M., and Platt, U.: Halogen oxide measurements at Masaya Volcano, Nicaragua using active long path differential optical absorption spectroscopy, B. Volcanol., 71, 659–670, 2009.
Kurosu, T. P., Chance, K., and Sioris, C. E.: Preliminary results for HCHO and BrO from the EOS-aura ozone monitoring instrument, in: Fourth International Asia-Pacific Environmental Remote Sensing Symposium 2004: Remote Sensing of the Atmosphere, Ocean, Environment, and Space, International Society for Optics and Photonics, 116–123, 2004.
Lee, C., Kim, Y. J., Tanimoto, H., Bobrowski, N., Platt, U., Mori, T., Yamamoto, K., and Hong, C. S.: High ClO and ozone depletion observed in the plume of Sakurajima volcano, Japan, Geophys. Res. Lett., 32, L21809, doi:10.1029/2005GL023785, 2005.
Lefèvre, J., Menkes, C., Bani, P., Marchesiello, P., Curci, G., Grell, G. A., and Frouin, R.: Distribution of sulfur aerosol precursors in the SPCZ released by continuous volcanic degassing

ACPD
15, 35313–35381, 2015

at Ambrym, Vanuatu, J. Volcanol. Geoth. Res., doi:10.1016/j.jvolgeores.2015.07.018, online first, 2015.

Li, C., Joiner, J., Krotkov, N. A., and Bhartia, P. K.: A fast and sensitive new satellite SO_2 retrieval algorithm based on principal component analysis: Application to the ozone monitoring instrument, Geophys. Res. Lett., 40, 6314–6318, doi:10.1002/2013GL058134, 2013.

Logan, J. A.: An analysis of ozonesonde data for the troposphere: Recommendations for testing 3-D models and development of a gridded climatology for tropospheric ozone, J. Geophys. Res., 104, 16115–16149, doi:10.1029/1998JD100096, 1999.

Longo, K. M., Freitas, S. R., Pirre, M., Marécal, V., Rodrigues, L. F., Panetta, J., Alonso, M. F., Rosário, N. E., Moreira, D. S., Gácita, M. S., Arteta, J., Fonseca, R., Stockler, R., Katsurayama, D. M., Fazenda, A., and Bela, M.: The Chemistry CATT-BRAMS model (CCATT-BRAMS 4.5): a regional atmospheric model system for integrated air quality and weather forecasting and research, Geosci. Model Dev., 6, 1389–1405, doi:10.5194/gmd-6-1389-2013, 2013.

Marécal, V., Pirre, M., Krysztofiak, G., Hamer, P. D., and Josse, B.: What do we learn about bromoform transport and chemistry in deep convection from fine scale modelling?, Atmos. Chem. Phys., 12, 6073–6093, doi:10.5194/acp-12-6073-2012, 2012.

Martin, R. S., Mather, T. A., and Pyle, D. M.: High-temperature mixtures of magmatic and atmospheric gases, Geochem. Geophy. Geosy., 7, Q04006, doi:10.1029/2005GC001186, 2006.

Martin, R. S., Roberts, T. J., Mather, T. A., and Pyle, D. M.: The implications of H_2S and H_2 kinetic stability in high-T mixtures of magmatic and atmospheric gases for the production of oxidized trace species (eg, BrO and NO_x), Chem. Geol., 263, 143–159, 2009.

Martin, R. S., Ilyinskaya, E., and Oppenheimer, C.: The enigma of reactive nitrogen in volcanic emissions, Geochim. Cosmochim. Ac., 95, 93–105, 2012.

Mather, T. A., Allen, A. G., Oppenheimer, C., Pyle, D. M., and McGonigle, A. J. S.: Size-resolved characterisation of soluble ions in the particles in the tropospheric plume of Masaya volcano, Nicaragua: origins and plume processing, J. Atmos. Chem., 46, 207–237, 2003.

Mather, T. A., Pyle, D. M., and Allen, A. G.: Volcanic source for fixed nitrogen in the early Earth's atmosphere, Geology, 32, 905–908, doi:10.1130/G20679.1, 2004.

Myhre, G., Shindell, D., Bréon, F.-M., Collins, W., Fuglestvedt, J., Huang, J., Koch, D., Lamarque, J.-F., Lee, D., Mendoza, B., Nakajima, T., Robock, A., Stephens, G., Takemura, H., and Zhang, T.: Anthropogenic and natural radiative forcing, in: Climate Change 2013: the Physical Science Basis, contribution of Working Group I to the Fifth Assessment Report of the

Intergovernmental Panel on Climate Change, edited by: Stocker, T. F., Qin, D., Plattner, G.-K., Tignor, M., Allen, S. K., Boschung, J., Nauels, A., Xia, Y., Bex, V., and Midgley, P. M., Cambridge University Press, Cambridge, UK and New York, NY, USA, 2013.

Naik, V., Voulgarakis, A., Fiore, A. M., Horowitz, L. W., Lamarque, J.-F., Lin, M., Prather, M. J., Young, P. J., Bergmann, D., Cameron-Smith, P. J., Cionni, I., Collins, W. J., Dalsøren, S. B., Doherty, R., Eyring, V., Faluvegi, G., Folberth, G. A., Josse, B., Lee, Y. H., MacKenzie, I. A., Nagashima, T., van Noije, T. P. C., Plummer, D. A., Righi, M., Rumbold, S. T., Skeie, R., Shindell, D. T., Stevenson, D. S., Strode, S., Sudo, K., Szopa, S., and Zeng, G.: Preindustrial to present-day changes in tropospheric hydroxyl radical and methane lifetime from the Atmospheric Chemistry and Climate Model Intercomparison Project (ACCMIP), Atmos. Chem. Phys., 13, 5277–5298, doi:10.5194/acp-13-5277-2013, 2013.

Oppenheimer, C., Tsanev, V. I., Braban, C. F., Cox, R. A., Adams, J. W., Aiuppa, A., Bobrowski, N., Delmelle, P., Barclay, J., and McGonigle, A. J. S.: BrO formation in volcanic plumes, Geochim. Cosmochim. Ac., 70, 2935–2941, 2006.

Oppenheimer, C., Kyle, P., Eisele, F., Crawford, J., Huey, G., Tanner, D., Kim, S., Maudlin, L., Blake, D., Beyersdorf, A., Bubr, M., and Davis, D.: Atmospheric chemistry of an Antarctic volcanic plume, J. Geophys. Res.-Atmos., 115, D04303, doi:10.1029/2009JD011910, 2010.

Popp, C., McCormick, B., Suleiman, R., Chance, K., Andrews, B., and Cottrell, E.: Analysis of volcanic bromine monoxide emissions in the southwestern Pacific region in 2005 based on satellite observations from OMI, Geophys. Res. Abstr., EGU2015-9837, EGU General Assembly 2015, Vienna, Austria, 2015.

Putirka, K. D.: Thermometers and barometers for volcanic systems, in: Minerals, Inclusions and Volcanic Processes, edited by: Putirka, K. D. and Tepley, F., Rev. Mineral. Geochem., 69, 61–120, 2008.

Pyle, D. M. and Mather, T. A.: Halogens in igneous processes and their fluxes to the atmosphere and oceans from volcanic activity: a review, Chem. Geol., 263, 110–121, 2009.

Roberts, T. J., Braban, C. F., Martin, R. S., Oppenheimer, C., Adams, J. W., Cox, R. A., Jones, R. L., and Griffiths, P. T.: Modelling reactive halogen formation and ozone depletion in volcanic plumes, Chem. Geol., 263, 151–163, 2009.

Roberts, T. J., Martin, R. S., and Jourdain, L.: Reactive bromine chemistry in Mount Etna's volcanic plume: the influence of total Br, high-temperature processing, aerosol loading and plume–air mixing, Atmos. Chem. Phys., 14, 11201–11219, doi:10.5194/acp-14-11201-2014, 2014a.

ACPD
15, 35313–35381, 2015

Roberts, T. J., Jourdain, L., Griffiths, P. T., and Pirre, M.: Re-evaluating the reactive uptake of HOBr in the troposphere with implications for the marine boundary layer and volcanic plumes, Atmos. Chem. Phys., 14, 11185–11199, doi:10.5194/acp-14-11185-2014, 2014b.

Roberts, T. J., Vignelles, D., Liuzzo, M., Giudice, G., Aiuppa, A., Chartier, M., Coute, B., Lurton, T., Berthet, G., and Renard, J.-B.: Advances in in-situ real-time monitoring of volcanic emissions: HCl, and size-resolved aerosol at Mt Etna (passive degassing), Geochim. Cosmochim. Ac., submitted, 2015.

Robin, C., Eissen, J.-P., and Monzier, M.: Giant tuff cone and 12-kin-wide associated caldera at Ambrym Volcano (Vanuatu, New Hebrides Arc), J. Volcanol. Geotherm. Res., 55, 225–238, 1993.

Roine, A.: HSC Chemistry 6.1, Tech. rep. Outotec Research Oy, Pori, Finland, 2007.

Rosário, N. E., Longo, K. M., Freitas, S. R., Yamasoe, M. A., and Fonseca, R. M.: Modeling the South American regional smoke plume: aerosol optical depth variability and surface shortwave flux perturbation, Atmos. Chem. Phys., 13, 2923–2938, doi:10.5194/acp-13-2923-2013, 2013.

Rotstayn, L. D. and Lohmann, U.: Simulation of the tropospheric sulfur cycle in a global model with a physically based cloud scheme, J. Geophys. Res., 107, 4592, doi:10.1029/2002JD002128, 2002

Saiz-Lopez, A., Plane, J. M. C., and Shillito, J. A.: Bromine oxide in the mid-latitude marine boundary layer, Geophys. Res. Lett., 31, L03111, doi:10.1029/2003GL018956, 2004.

Sander, R.: Compilation of Henry's Law Constants for Inorganic and Organic Species of Potential Importance in Environmental Chemistry, available at: http://www.henrys-law.org/henry-3.0.pdf (last access: November 2015), 1999.

Sander, S. P., Friedl, R. R., Golden, D. M., Kurylo, M. J., Moortgat, G. K., Keller-Rudek, H., Wine, P. H., Ravishankara, A. R., Kolb, C. E., Molina, M. J., Finlayson-Pitts, B. J., Huie, R. E., and Orkin, V. L.: Chemical Kinetics and Photochemical Data for Use in Atmospheric Studies, Evaluation Number 15, JPL Publication 06-2, Jet Propulsion Laboratory, Pasadena, CA, available at: http://jpldataeval.jpl.nasa.gov/pdf/JPL_15_AllInOne.pdf (last access: November 2015), 2006.

Schmidt, A., Carslaw, K. S., Mann, G. W., Wilson, M., Breider, T. J., Pickering, S. J., and Thordarson, T.: The impact of the 1783–1784 AD Laki eruption on global aerosol formation processes and cloud condensation nuclei, Atmos. Chem. Phys., 10, 6025–6041, doi:10.5194/acp-10-6025-2010, 2010.

ACPD
15, 35313–35381, 2015

Schmidt, A., Carslaw, K. S., Mann, G. W., Rap, A., Pringle, K. J., Spracklen, D. V., Wilson, M., and Forster, P. M.: Importance of tropospheric volcanic aerosol for indirect radiative forcing of climate, Atmos. Chem. Phys., 12, 7321–7339, doi:10.5194/acp-12-7321-2012, 2012.

Schultz, M., Backman, L., Balkanski, Y., Bjoerndalsaeter, S., Brand, R., Burrows, J., Dalsoeren, S., de Vasconcelos, M., Grodtmann, B., Hauglustaine, D., Heil, A., Hoelzemann, J., Isaksen, I., Kaurola, J., Knorr, W., Ladstaetter-Weienmayer, A., Mota, B., Oom, D., Pacyna, J., Panasiuk, D., Pereira, J., Pulles, T., Pyle, J., Rast, S., Richter, A., Savage, N., Schnadt, C., Schulz, M., Spessa, A., Staehelin, J., Sundet, J., Szopa, S., Thonicke, K., van het Bolscher, M., van Noije, T., van Velthoven, P., Vik, A., and Wittrock, F.: REanalysis of the TROpospheric Chemical Composition Over the Past 40 years (RETRO). A Long-Term Global Modeling Study of Tropospheric Chemistry, Final Report, Tech. rep., Max Planck Institute for Meteorology, Hamburg, Germany, 2007.

Schumann, U., Weinzierl, B., Reitebuch, O., Schlager, H., Minikin, A., Forster, C., Baumann, R., Sailer, T., Graf, K., Mannstein, H., Voigt, C., Rahm, S., Simmet, R., Scheibe, M., Lichtenstern, M., Stock, P., Rüba, H., Schäuble, D., Tafferner, A., Rautenhaus, M., Gerz, T., Ziereis, H., Krautstrunk, M., Mallaun, C., Gayet, J.-F., Lieke, K., Kandler, K., Ebert, M., Weinbruch, S., Stohl, A., Gasteiger, J., Groß, S., Freudenthaler, V., Wiegner, M., Ansmann, A., Tesche, M., Olafsson, H., and Sturm, K.: Airborne observations of the Eyjafjalla volcano ash cloud over Europe during air space closure in April and May 2010, Atmos. Chem. Phys., 11, 2245–2279, doi:10.5194/acp-11-2245-2011, 2011.

Seinfeld, J. H. and Pandis, A. N.: Properties of the atmospheric aerosol, in: Atmospheric Chemistry and Physics – from Air Pollution to Climate Change, Chapter 8, John Wiley and Sons, New Jersey, USA, 350–394, 2006.

Sheehan, F. and Barclay, J.: Staged storage and magma recycling at Ambrym volcano, Vanuatu, J. Volcanol. Geoth. Res., submitted, 2015.

Siebert, L., Simkin, T., and Kimberly, P.: Volcanoes of the World, 3rd Edn., Berkeley: University of California Press, United States of America, 568 pp., 2010.

Simpson, W. R., Brown, S. S., Saiz-Lopez, A., Thornton, J. A., and von Glasow, R.: Tropospheric halogen chemistry: sources, cycling, and impacts, Chem. Rev., 115, 4035–4062, doi:10.1021/cr5006638, 2015.

Stevenson, D. S., Johnson, C. E., Collins, W. J., and Derwent, R. G.: The tropospheric sulphur cycle and the role of volcanic SO_2, Geol. Soc. Spec. Publ., 213, 295–305, 2003.

ACPD
15, 35313–35381, 2015

Stockwell, W. R., Kirchner, F., Kuhn, M., and Seefeld, S.: A new mechanism for regional atmospheric chemistry modeling, J. Geophys. Res.-Atmos., 102, 25847–25879, 1997.

Surl, L., Donohoue, D., Aiuppa, A., Bobrowski, N., and von Glasow, R.: Quantification of the depletion of ozone in the plume of Mount Etna, Atmos. Chem. Phys., 15, 2613–2628, doi:10.5194/acp-15-2613-2015, 2015.

Tabazadeh, A., Toon, O. B., Clegg, S. L., and Hamill, P.: A new parameterization of H_2SO_4/H_2O aerosol composition: atmospheric implications, Geophys. Res. Lett., 24, 1931–1934, 1997.

Theys, N., Van Roozendael, M., Dils, B., Hendrick, F., Hao, N., and De Maziere, M.: First satellite detection of volcanic bromine monoxide emission after the Kasatochi eruption, Geophys. Res. Lett., 36, L03809, doi:10.1029/2008GL036552, 2009.

Tie, X., Madronich, S., Walters, S., Zhang, R., Rasch, P., and Collins, W.: Effect of clouds on photolysis and oxidants in the troposphere, J. Geophys. Res.-Atmos., 108, 4642, doi:10.1029/2003JD003659, 2003.

van der Werf, G. R., Randerson, J. T., Giglio, L., Collatz, G. J., Kasibhatla, P. S., and Arellano Jr., A. F.: Interannual variability in global biomass burning emissions from 1997 to 2004, Atmos. Chem. Phys., 6, 3423–3441, doi:10.5194/acp-6-3423-2006, 2006.

Vance, A., McGonigle, A. J. S., Aiuppa, A., Stith, J. L., Turnbull, K., and von Glasow, R.: Ozone depletion in tropospheric volcanic plumes, Geophys. Res. Lett., 37, L22802, doi:10.1029/2010GL044997, 2010.

Voigt, C., Jessberger, P., Jurkat, T., Kaufmann, S., Baumann, R., Schlager, H., Bobrowski, N., Giuffrida, G., and Salerno, G.: Evolution of CO_2, SO_2, HCl, and HNO_3 in the volcanic plumes from Etna, Geophys. Res. Lett., 41, 2196–2203, 2014.

von Glasow, R.: Atmospheric chemistry in volcanic plumes, P. Natl. Acad. Sci. USA, 107, 6594–6599, 2010.

von Glasow, R., Bobrowski, N., and Kern, C.: The effects of volcanic eruptions on atmospheric chemistry, Chem. Geol., 263, 131–142, 2009.

Walko, R. L., Band, L. E., Baron, J., Kittel, T. G. F., Lammers, R., Lee, T. J., Ojima, D., Pielke Sr., R. A., Tayloer, C., Tague, C., Tremback, C. J., and Vidale, P. L.: Coupled atmosphere-biophysics-hydrology models for environmental modeling, J. Appl. Meteorol., 39, 931–944, 2000.

Wang, T. X., Kelley, M. D., Cooper, J. N., Beckwith, R. C., and Margerum, D. W.: Equilibrium, kinetic, and UV-spectral characteristics of aqueous bromine chloride, bromine, and chlorine species, Inorg. Chem., 33, 5872–5878, 1994.

ACPD
15, 35313–35381, 2015

Table 1. Heterogeneous reactions in the model and their associated reactive uptake coefficients on sulfate aerosol. See Sect. 2.3.1 for description of the calculation of the ratio $\frac{[BrCl_{(aq)}]}{[Br_{2\,(aq)}]}$.

Reaction	Reactive uptake coefficient
$HOBr + H^+_{(aq)} + Br^-_{(aq)} \rightarrow Br_{2(aq\rightarrow g)} + H_2O$	$0.2 \times \frac{[Br_{2\,(aq)}]}{[Br_{2\,(aq)}]+[BrCl_{(aq)}]}$
$HOBr + H^+_{(aq)} + Cl^-_{(aq)} \rightarrow BrCl_{(aq\rightarrow g)} + H_2O$	$0.2 \times \frac{[BrCl_{\,(aq)}]}{[Br_{2\,(aq)}]+[BrCl_{(aq)}]}$
$BrONO_2 + H_2O \rightarrow HOBr_{(aq\rightarrow g)} + HNO_3$	0.8

ACPD
15, 35313–35381, 2015

Table 2. SO_2 emission rates in January 2005 from the principal active Vanuatu's volcanoes (Gaua, Aoba, Lopevi, Epi, Ambrym, Yasur) as prescribed in the simulations. Details for each volcano are given in the following: (a) in Bani et al. (2012), only information during a phase of eruptive activity. We prescribed the post eruptive degassing rate (for the volcanoes that had an eruption since 1900) of 0.070 kt day^{-1} assigned for this volcano in the AEROCOM database. (b) Before eruption of November 2005, no significant passive degassing. We prescribed the post eruptive degassing rate of 0.070 kt day^{-1} assigned in the AEROCOM database. (c) Mean of 5 transverses of 12 January 2005 in Bani et al. (2012). Note that, in the fourth grid, the two Marum and Benbow cones do not lie in the same gridbox. As a result, we prescribed 60 % of the emission in the model gridbox containing Marum and 40 % in the gridbox containing Benbow as found in Bani et al. (2009). Note, that in the AEROCOM database, the value is 0.0807 kt day^{-1}. (d) Lopevi is a volcano with frequent degassing. From Bani et al. (2006), vapor was observed covering the crater but it was difficult to conclude on its volcanic activy. Local observers in Vanuatu indicated ongoing eruptive activity at Lopevi starting at the end of January 2005 and continuing on February (GPV). Mean of 3 traverses of passive degassing of 24 February 2006 was 0.156 kt day^{-1}. As a result, we kept the value of AEROCOM database of 0.070 kt day^{-1}. (e) No information. Post eruptive degassing rate of 0.070 kt day^{-1} is assigned in AEROCOM database. (f) Value of 10 January 2005 of Bani et al. (2012). In AEROCOM database, it is 0.900 kt day^{-1}.

Volcano	Reported activity	Emission (kt day^{-1})	Source
Gaua	None	0,070 kt day^{-1}	AEROCOM database (a)
Aoba (Ambae)	None	0.070 kt day^{-1}	AEROCOM database (b)
Ambrym	Extreme passive degassing	18.835 kt day^{-1}	Bani et al. (2012) (c)
Lopevi	Not clear	0.070 kt day^{-1}	Bani et al. (2012) (d)
Epi	None	0.070 kt day^{-1}	AEROCOM database (e)
Yasur	Eruption	0.968 kt day^{-1}	Bani et al. (2012) (f)

ACPD
15, 35313–35381, 2015

Table 3. Composition inputs to the HSC Chemistry model assuming plume-air mixture of 98 : 2 magmatic : atmospheric gases, with temperatures 1125 and 20 °C, resulting in mixed temperature of 1103 °C. Resulting output of the HSC Chemistry simulations were converted to ratios relative to sulfur and used to initialize the S1_HighT model simulation (second row of Table 4). The HSC Chemistry model is presented in Sect. 2.3.3.

Gas	Mixing ratio in HSC input
H_2O	9.29×10^{-1}
N_2	1.56×10^{-2}
CO_2	3.80×10^{-2}
SO_2	1.05×10^{-2}
HCl	1.84×10^{-3}
O_2	4.20×10^{-3}
Ar	2.00×10^{-4}
HBr	7.23×10^{-6}
HF	7.53×10^{-4}

ACPD
15, 35313–35381, 2015

Table 4. Emissions of HCl, HBr, sulfate and radicals (Cl, Br, OH, NO) expressed in terms of mass ratios relative to SO_2 emissions for all the volcanoes within the domain study and for the different simulations (see Sect. 2.3.4 for details on the simulations). S1_no_hal, S1_no_hal2 and S0 have the same emissions than S1_HighT except for Ambrym volcano whose emission in theses simulations is indicated in the table. Note that all the simulations, except S0, have an emission of SO_2 for Ambrym of 18.8 kt day^{-1} and a sulfate aerosol emission (1 % of sulfur (= $SO_2 + H_2SO_4$)). S0 does not include any volcanic emissions from Ambrym.

Simulations	HCl/SO_2	HBr/SO_2	H_2SO_4/SO_2	Cl/SO_2	Br/SO_2	OH/SO_2	NO/SO_2
S1	0.1	8.75×10^{-4}	1.55×10^{-2}	0	0	0	0
S1_HighT	0.1	6.87×10^{-4}	1.55×10^{-2}	1.33×10^{-4}	1.89×10^{-4}	7.04×10^{-4}	7.45×10^{-4}
S1_HighT_no NO_x	0.1	6.87×10^{-4}	1.55×10^{-2}	1.33×10^{-4}	1.89×10^{-4}	7.04×10^{-4}	0
S1_no_hal Ambrym only	0	0	0	0	0	0	0
S1_no_hal2 Ambrym only	0	0	0	0	0	7.04×10^{-4}	0
S0 Ambrym only	0	0	0	0	0	0	0

ACPD
15, 35313–35381, 2015

Table 5. Statistical comparison between DOAS SO_2 and BrO columns and the corresponding simulated values (for S1 and S1_HighT). Correlation coefficients (r), root mean square error (RMSE in molecule cm^{-2}) are given as well as mean values (molecule cm^{-2}) of observed and simulated data. Note that we did not include here the data for which we did not have GPS data (dashed lines of Figs. 3 and 4).

	Mean SO_2	Mean BrO	r_{SO_2}	r_{BrO}	$RMSE_{SO_2}$	$RMSE_{BrO}$
DOAS	2.29×10^{18}	5.84×10^{14}				
S1	2.27×10^{18}	1.14×10^{14}	0.62	−0.21	1.09×10^{18}	5.97×10^{14}
S1_HighT	2.25×10^{18}	3.42×10^{14}	0.61	0.59	1.10×10^{18}	3.90×10^{14}

ACPD
15, 35313–35381, 2015

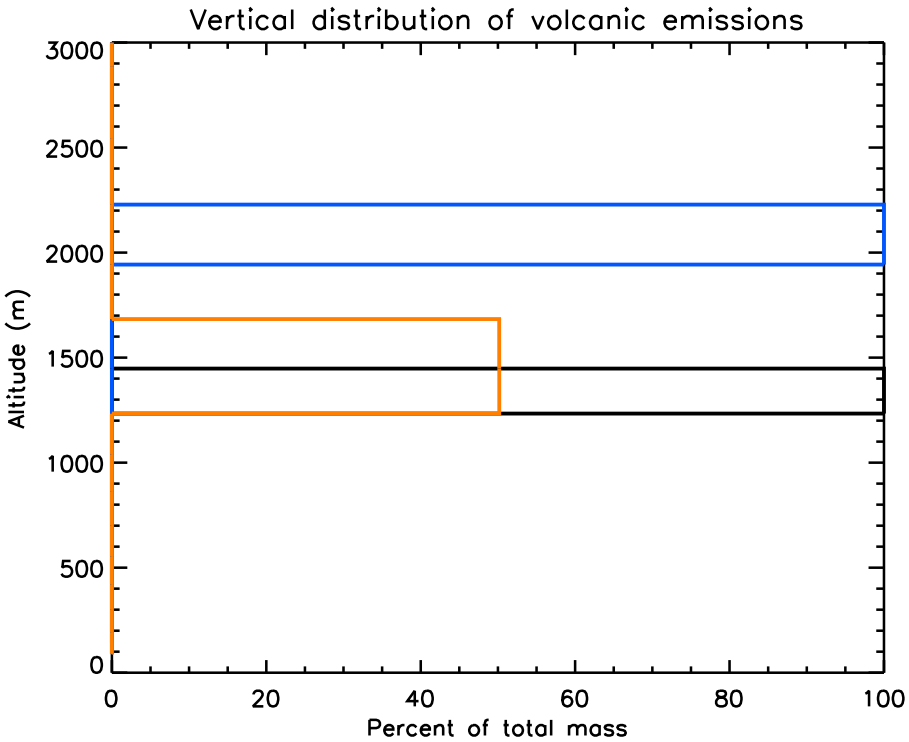

Figure 1. Vertical distribution of volcanic emissions from Ambrym as prescribed in the model for the all the simulations (black line) except for the sensitivity simulations S1_HighT_alt (blue line), S1_HighT_width (orange line). See Sect. 2.3.4 for details on simulations.

ACPD
15, 35313–35381, 2015

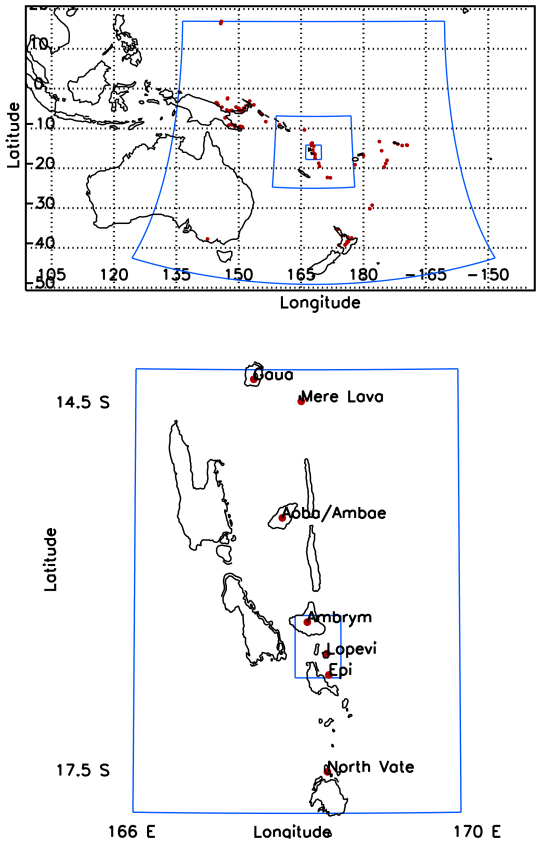

Figure 2. Top: position of the nested model grids (blue lines) and of the volcanoes (red filled circles) taken into account in the simulations. For clarity, only the 3 largest model grids are shown. Bottom: zoom on the two smallest model grids (blue lines) and on the volcanoes (red filled circles) taken into account in the simulations. Resolution of each grid is given in Sect. 2.3.4.

ACPD
15, 35313–35381, 2015

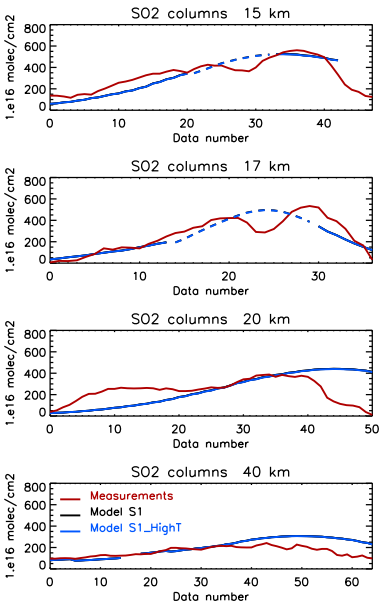

Figure 3. Comparison between SO_2 columns observed by Bani et al. (2009) (red line) and simulated by the model for S1 (black line), S1_HighT (blue line). Each panel represents a traverse of the Ambrym plume in the cross-wind direction on the 12 January 2005 between 05:00 and 06:00 UT, at a range of distances downwind. The x axis shows the datapoint number in the transect across the plume (Bani et al., 2009). The direction of each transect across the plume has a east–west component. Here, each transect is shown with the datapoints from west to east (left to right). Note that model results are for the same position and time as the measurements and for the finest grid (0.5 km × 0.5 km) except when GPS data (longitude and latitude) were not available. In this case, model results (dashed lines) were interpolated between the last and the next positions for which we had GPS data. Note that black and blue lines are on top of each other (superimposed). Reported error from DOAS measurements (1σ) is 2.45×10^{16} molecule cm^{-2}.

ACPD
15, 35313–35381, 2015

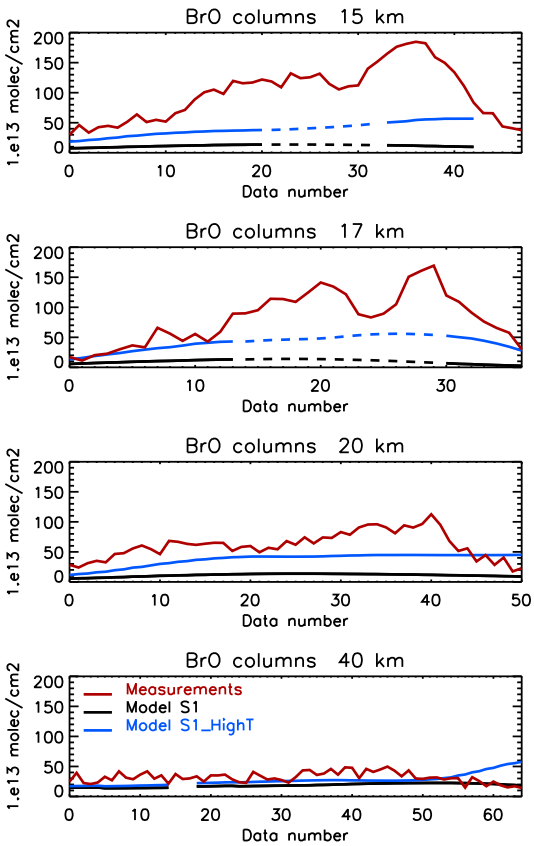

Figure 4. Comparison between BrO columns observed by Bani et al. (2009) (red line) and simulated by the model for S1 (black line), S1_HighT (blue line). See Fig. 3 for details on the method of comparison. Reported error (1σ) is 12.22×10^{13} molecule cm^{-2}.

ACPD
15, 35313–35381, 2015

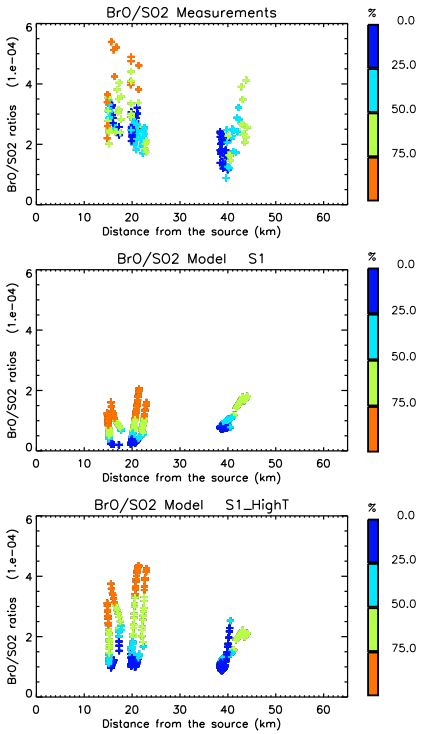

Figure 5. Variation of BrO/SO_2 ratios with distance from the vent derived from observations (top) and model simulations S1 (middle), S1_HighT(bottom) presented in Figs. 3 and 4. For each transect, each BrO/SO_2 ratio has been colored according to its SO_2 column value relative to the maximal value of the SO_2 column (SO_2_max) for this transect. More precisely, the color indicates the relative difference $\frac{(SO_2\_max - SO_2)}{SO_2\_max}$. Note that we did not include the observations nor the corresponding model results for which we did not have GPS data (dashed lines of Figs. 3 and 4).

ACPD
15, 35313–35381, 2015

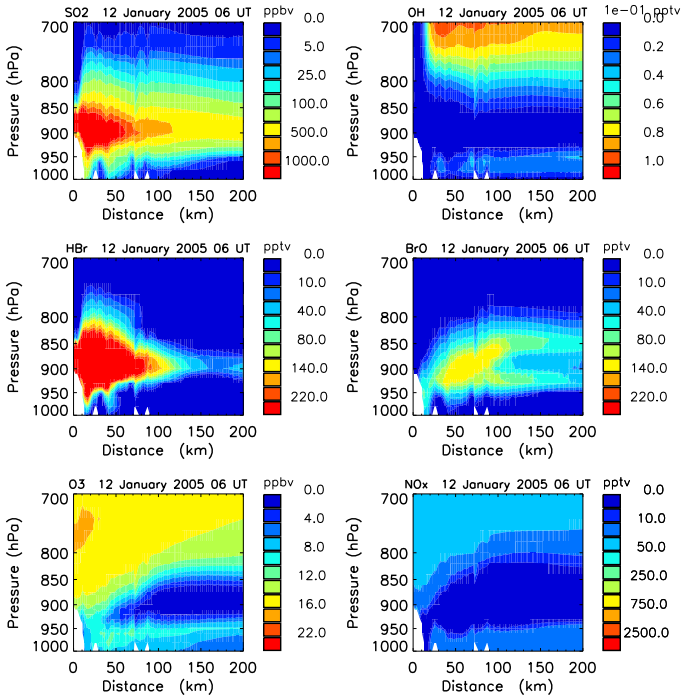

Figure 6. Distance–pressure cross section of the SO_2, OH, HBr, BrO, O_3 and NO_x mixing ratios in the plume of Ambrym on 12 January 2005 at 06:00 UT in the simulation S1.

ACPD
15, 35313–35381, 2015

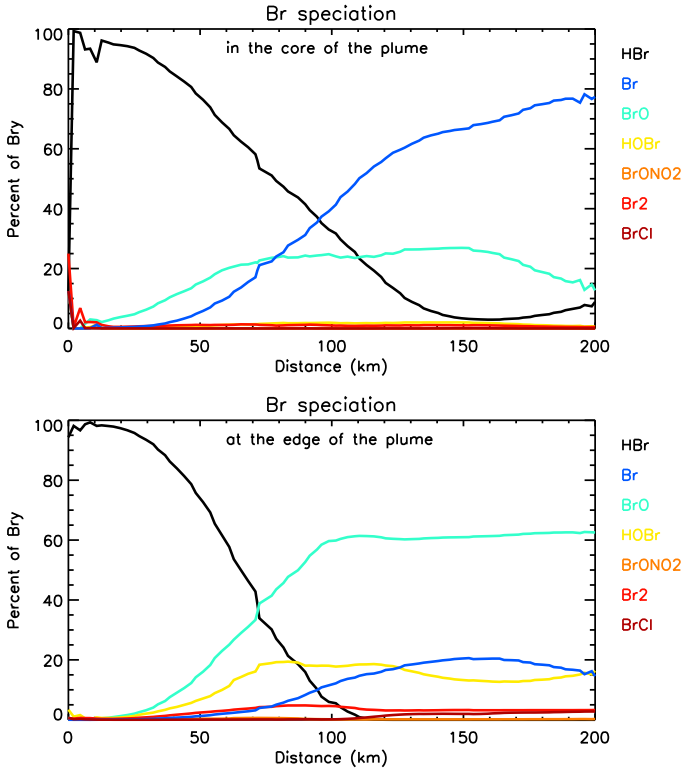

Figure 7. Br speciation along the plume (in the core and at the edge) in the simulation S1 and the grid 2 km × 2 km the 12 January 2005 at 06:00 UT. The Br speciation has been calculated as the percent of Br_y ($Br_y = HBr + 2Br_2 + BrCl + Br + BrO + HOBr + BrONO_2$). Distance is calculated from the middle of the gridbox containing Marum and Benbow.

ACPD
15, 35313–35381, 2015

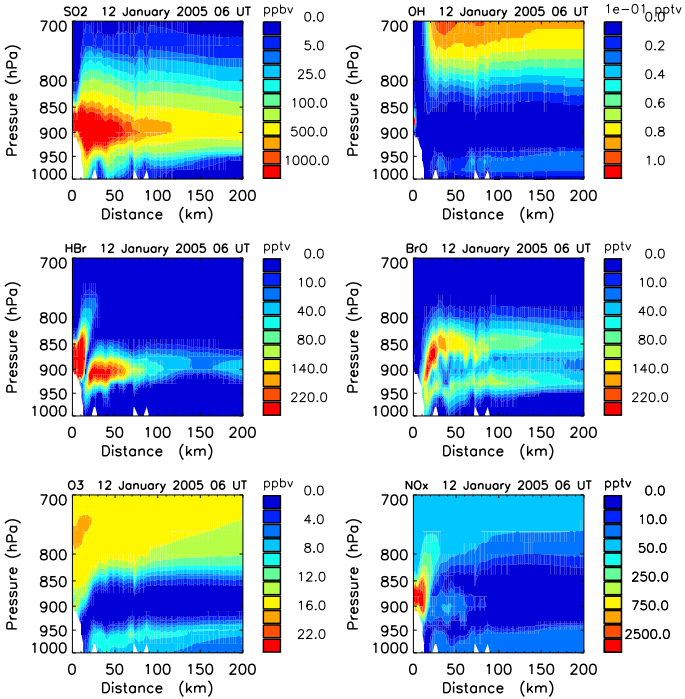

Figure 8. Distance–pressure cross section of the SO_2, OH, HBr, BrO, O_3 and NO_x mixing ratios in the plume of Ambrym on 12 January 2005 at 06:00 UT in the simulation S1_HighT.

ACPD
15, 35313–35381, 2015

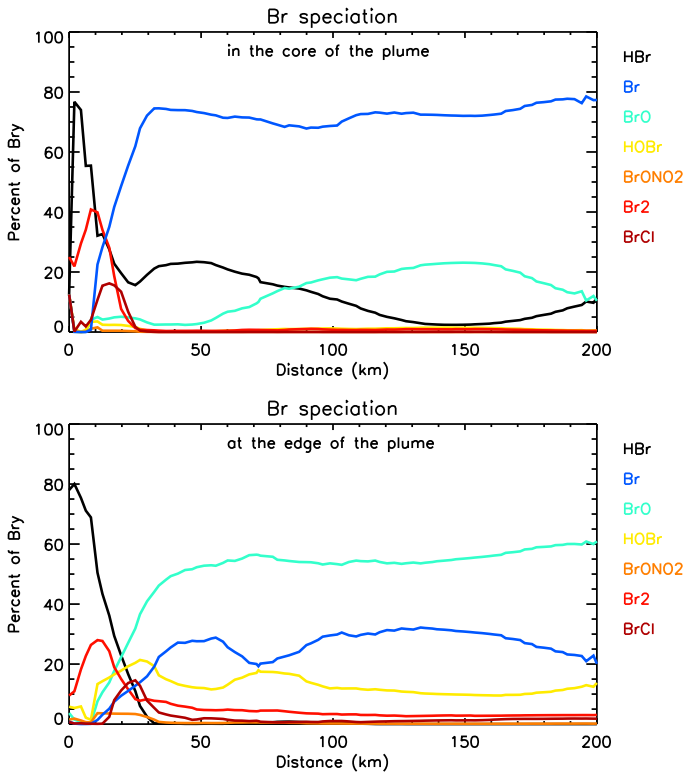

Figure 9. Br speciation along the plume (in the core and at the edge) in the simulation S1_HighT and the grid 2 km × 2 km the 12 January 2005 at 06:00 UT. The Br speciation has been calculated as the percent of Br_y ($Br_y = HBr + 2Br_2 + BrCl + Br + BrO + HOBr + BrONO_2$). Distance is calculated from the middle of the gridbox containing Marum and Benbow.

ACPD
15, 35313–35381, 2015

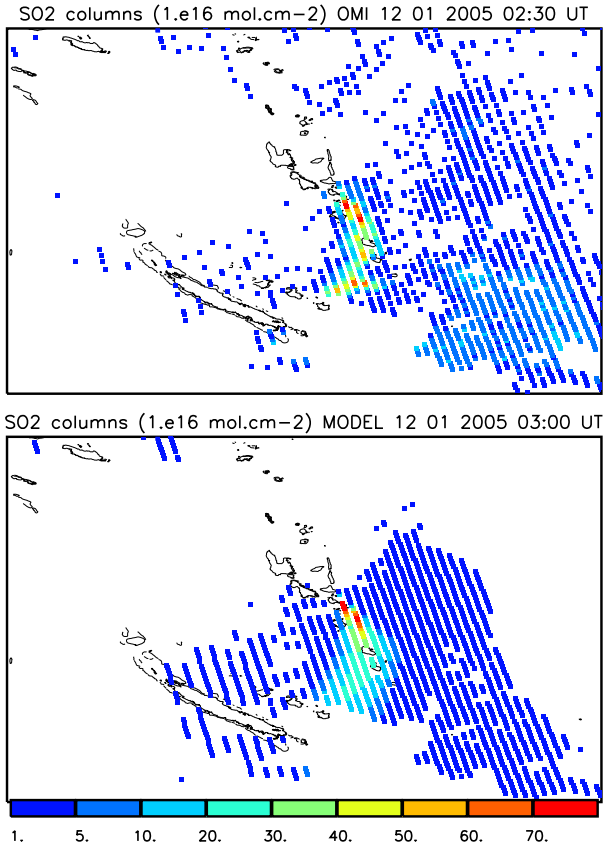

Figure 10. Top: OMI SO_2 columns (1×10^{16} molecule cm^{-2}) for the 12 January 2005 at 02:30 UT. Bottom: simulated SO_2 columns (1×10^{16} molecule cm^{-2}) (S1_HighT) from the grid 10 km × 10 km for the 12 January 2005 at 03:00 UT interpolated onto the OMI grid.

ACPD
15, 35313–35381, 2015

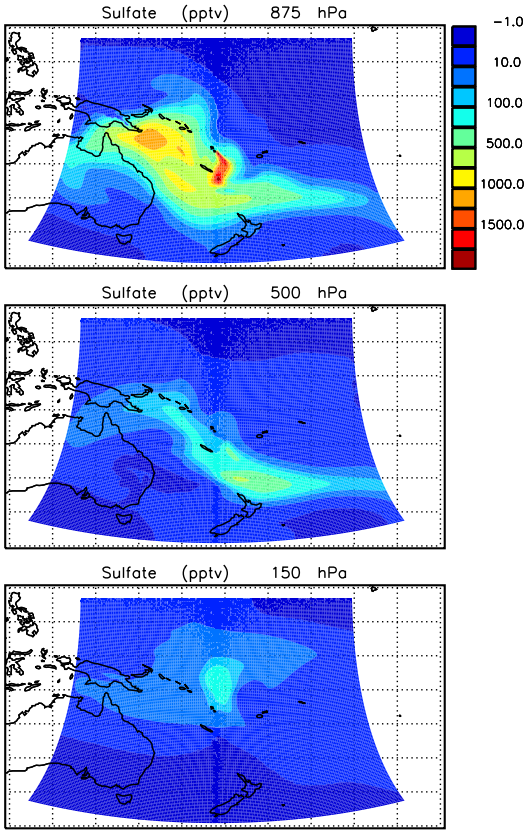

Figure 11. Daily mean difference (12 January 2005) between simulated sulfate in S1_HighTand in S0 at 875, 500 and 150 hPa for the grid 50 km × 50 km.

ACPD
15, 35313–35381, 2015

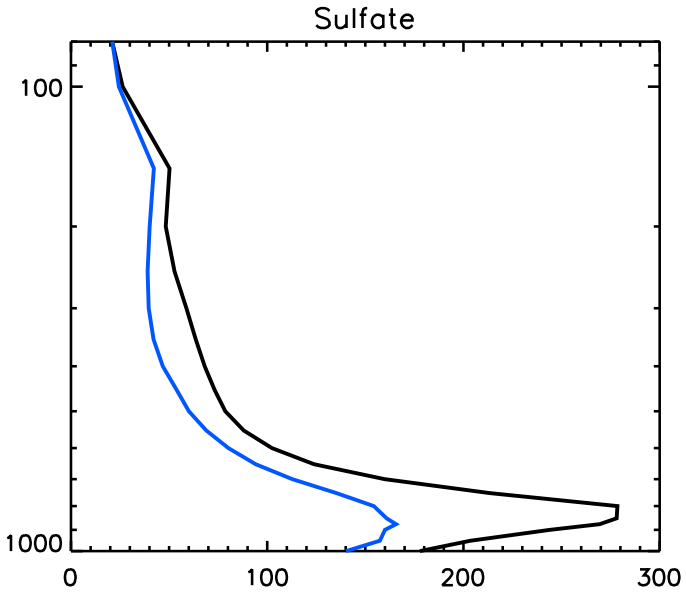

Figure 12. Profile of the daily (12 January 2005) mean mixing ratios of sulfate simulated by the model in the larger grid (of resolution 50 km × 50 km) in S1_HighT (black) and in S0 (light blue).

ACPD
15, 35313–35381, 2015

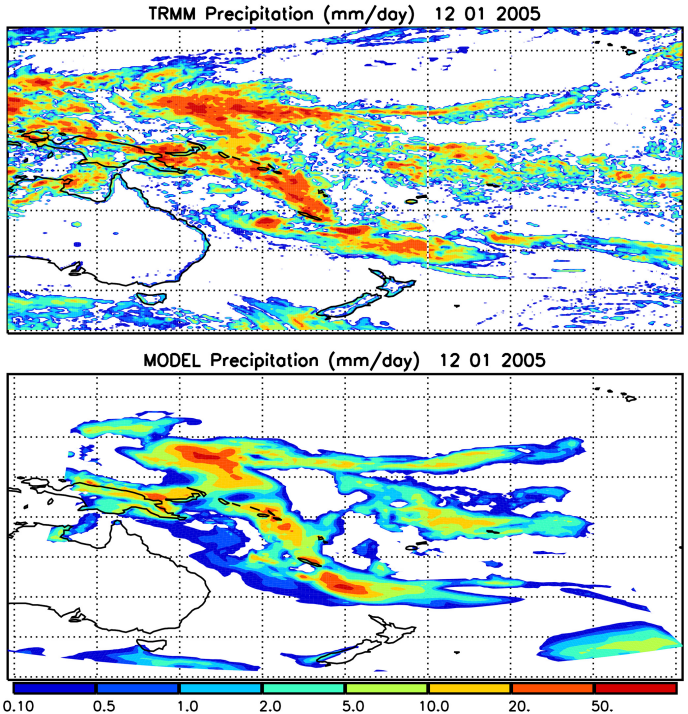

Figure 13. Daily precipitation (mm day^{-1}) for the 12 January 2005 as estimated from the TRMM satellite (3B42 product) and simulated by the model.

ACPD
15, 35313–35381, 2015

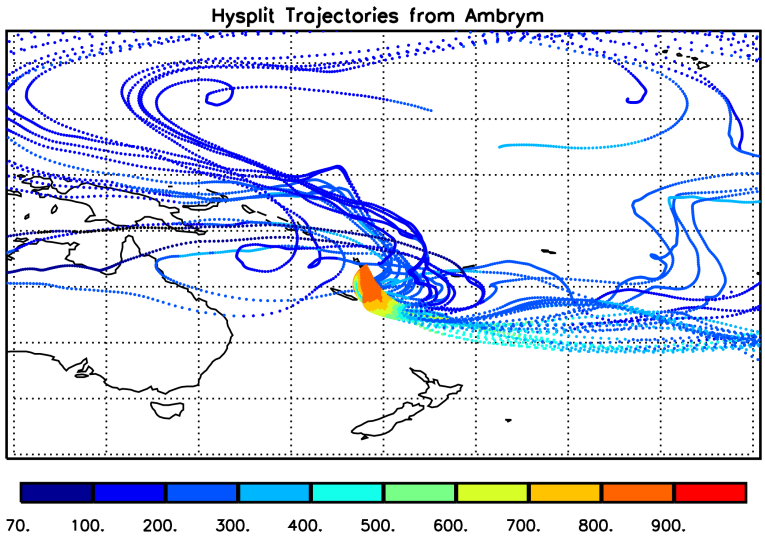

Figure 14. Fifteen-days forward trajectories initialized from the location of Ambrym volcano at 1373 m every hour on the 10 and 11 January 2005 calculated with the HYSPLIT model. The color scale represents the pressure of the air masses along the trajectories.

ACPD
15, 35313–35381, 2015

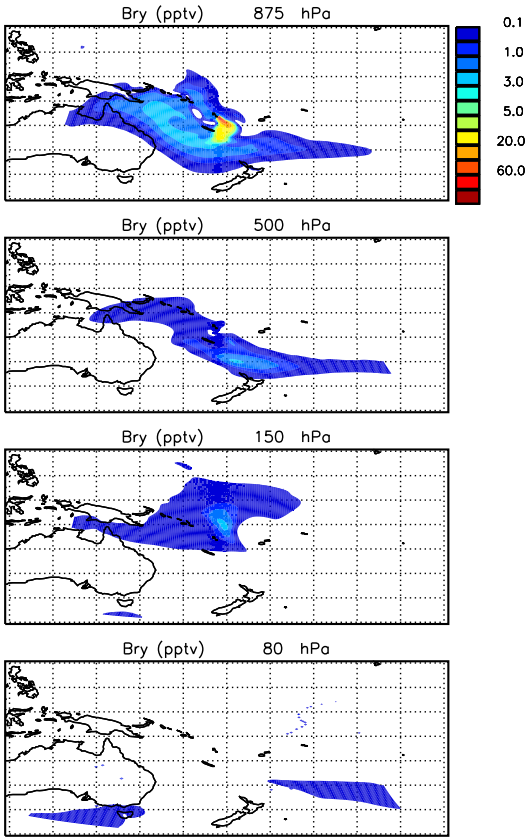

Figure 15. Daily mean difference (12 January 2005) between simulated Br_y (pptv) in S1_HighT and in S0 at 875, 500, 150 and 80 hPa for the 50 km × 50 km grid.

ACPD
15, 35313–35381, 2015

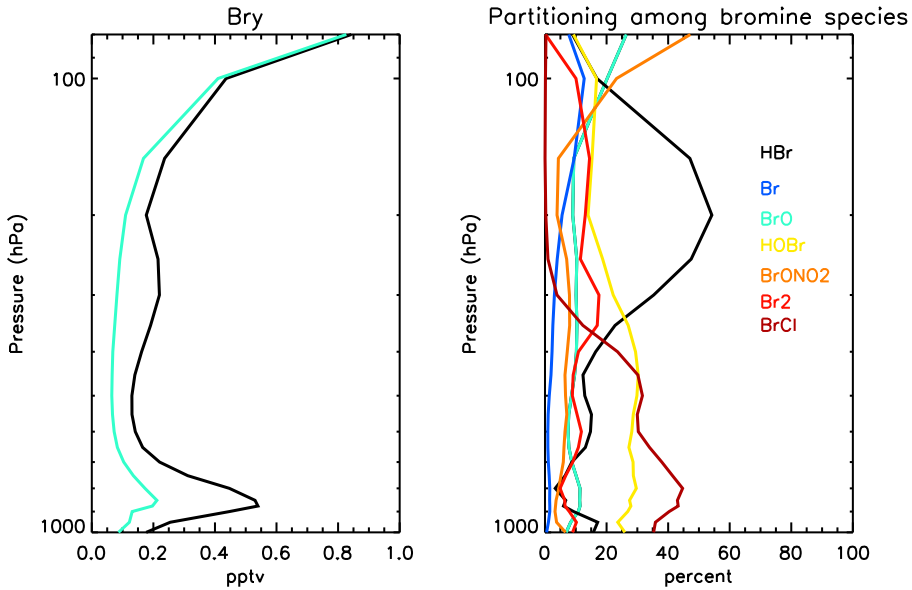

Figure 16. Left: profile of the daily (12 January 2005) mean mixing ratios of Br_y simulated by the model in the larger grid (50 km × 50 km) in S1_HighT (black) and in S0 (light blue). Right: daily mean (12 January 2005) of the Br speciation (%) for the simulation S1_HighT for grid boxes where Br_y mean difference between S1_HighT and S0 is larger than 0.5 pptv (Fig. 15).

ACPD
15, 35313–35381, 2015

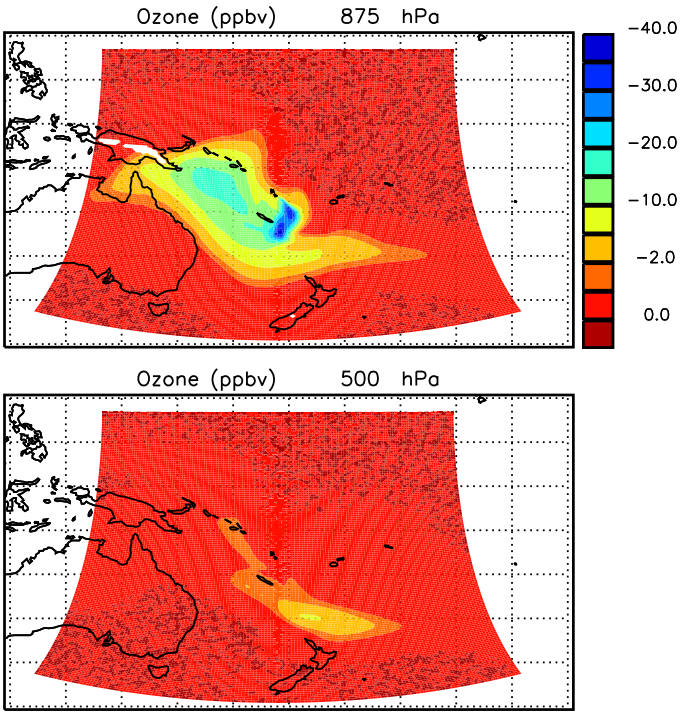

Figure 17. Daily mean difference (12 January 2005) between simulated ozone (%) in S1_HighT and in S0 at 875, 500 hPa for the 50 km × 50 km grid.

ACPD
15, 35313–35381, 2015